General Relativity and Gravitation, Vol. 36, No. 10, October 2004 (© 2004)

OPTIS—An Einstein Mission for Improved Tests of Special and General Relativity

C. Lämmerzahl,[1] I. Ciufolini,[2] H. Dittus,[1] L. Iorio,[3] H. Müller,[4] A. Peters,[4] E. Samain,[5] S. Scheithauer,[1] and S. Schiller[6] **A10**

Received March 23, 2004

The mission OPTIS aims at improving tests of the *foundations of Special and General Relativity* by up to three orders of magnitude. The individual tests concern

- the isotropy and
- constancy of the speed of light,
- the time dilation (or Doppler effect),
- the universality of the gravitational redshift with various combinations of high precision clocks. Furthermore, laser tracking and a laser link allows
- a strongly improved measurement of the gravitomagnetic Lense–Thirring effect,
- of the gravitoelectric Einstein perigee advance,
- of the gravitational redshift, and
- a search for deviations from Newtonian gravity.

For this mission, technologies are required which have been used recently to carry through the most precise tests of Special Relativity. The precision of these tests can be further increased under space conditions thanks to longer integration times, larger changes in the orbital velocity, and larger differences of the gravitational potential. Furthermore, very precise laser tracking and linking of satellites is a well established technique and will provide, in combination with the active drag–free control system, very accurate orbit data. The core technologies for OPTIS are optical cavities, highly stabilized lasers, capacitive gravitational reference sensors, drag–free control, ion clocks,

[1] ZARM, University Bremen, 28359 Bremen, Germany; e-mail: laemmerzahl@zarm.uni-bremen.de
[2] Dipartimento di Ingegneria dell' Innovazione dell' Università di Lecce and INFN Sezione di Lecce, via Monteroni, 73100, Lecce, Italy
[3] Dipartimento di Fisica dell' Università di Bari, via Amendola 173, 70126, Bari, Italy.
[4] Institute for Physics, Humboldt University, 10117 Berlin, Germany.
[5] Observatoire de la Côte Azur, 2130 Route de l'Observatoire, 06460 Caussols, France.
[6] Institut für Experimentalphysik, Heinrich–Heine–Universität Düsseldorf, 40225 Düsseldorf, Germany.

0001-7701/04/1000-2373/0

frequency combs, and laser tracking systems.
These technologies are also key technologies for other future missions.

KEY WORDS: Special Relativity; General Relativity; constancy of speed of light; gravitational redshift; Lense–Thirring effect; laser ranging; time transfer.

1. INTRODUCTION

Special Relativity (SR) and General Relativity (GR) are two of the most important theories of modern physics, see Fig. 1. These theories not only describe physical phenomena like the propagation of light or the gravitational interaction, they also present the formal frame for other theories like the Standard Model. They are basic for our understanding of space and time and thus for the underlying physical structure of any other theory. Last but not least, these theories have very important applications in science and even in every day life. Just to mention a few examples for the latter: Without taking into account SR, the Global Positioning System (GPS) makes errors of about 2 km per day and without GR even up to 10 km per day. SR as well as GR are also highly important for metrology. SR, with its statement about the constancy of the speed of light, provides the foundation for the current definition of length in terms of distance travelled by light within the $299\,792\,458^{\text{th}}$ part of a second. Furthermore, the independence of the time dilation effect from the nature of the used clocks is indispensable for a unique time–keeping in moving frames. Without GR, the universality of time–keeping in gravitational fields (which cannot be switched off) would be lost, implying a much more complicated and also less accurate definition of time, see Fig. 2. Needless to say, SR and GR are essential in the interpretation of astrophysical and cosmological data and also for the functioning and interpretation of high-energy physics experiments. Other important applications of SR and GR are telecommunication and geodesy. As a final point, we mention that the structure of present standard physical theories is such that any deviation from the standard laws like the Maxwell or Dirac equation (or, more generally, the Standard Model of elementary particle physics) will lead to deviations from SR and GR.

The most basic and puzzling features of SR and GR are their *universality principles*: For SR we have the universality of the speed of light, that is, its independence from the orientation and state of motion of the laboratory. Within the Mansouri–Sexl test theory, this has to be completed with a specific result of time-dilation experiments in order to uniquely derive SR. SR is an extremely well tested theory, however, given its basic role in any fundamental theory of physics, all its aspects, such as the already mentioned isotropy of speed of light, independence of speed of light from the velocity of the laboratory, and time dilation should be further tested as accurately as possible by current technology.

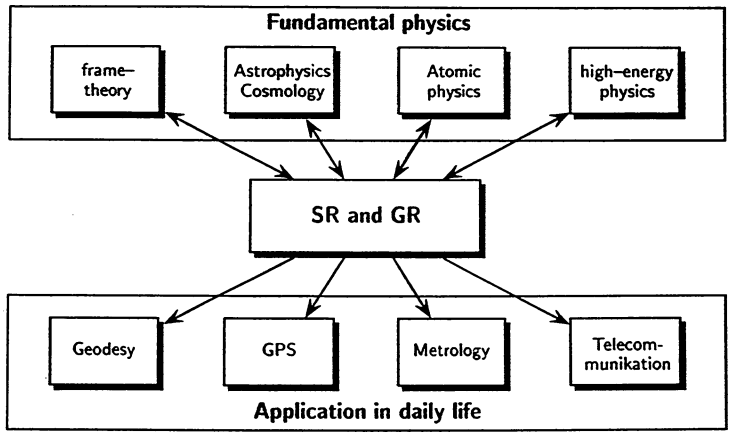

Figure 1. The importance of GR and SR in fundamental physics and in daily life. These theories not only represent a formal frame for all other physical theories but are also necessary in the exploration of the physics of the universe as for the interpretation of atomic and high–energy experiments. Furthermore, some techniques of daily life importance are heavily relying on SR and GR.

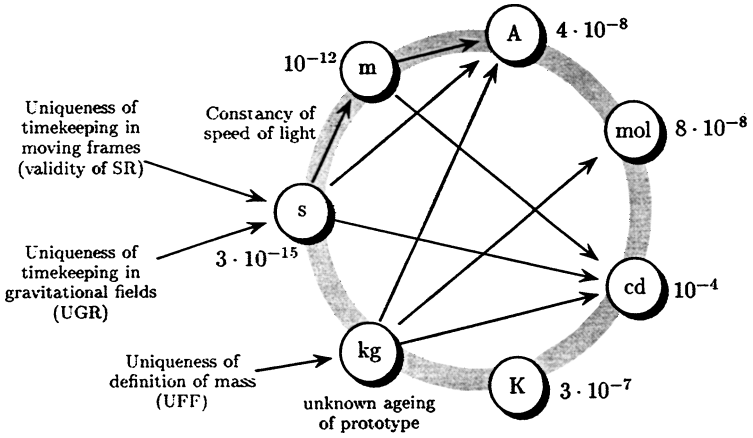

Figure 2. The SI–units (s = second, m = meter, A = Ampere, mol = mole, cd = candelas, K = Kelvin, kg = kilogram) and their interdependences [1]. The numbers indicate the stability of the corresponding unit. The uniqueness of the transport of the definition of the second and of the meter depends on the validity of the EEP. A replacement of the mechanical definition of the Ampere or other quantities also requires conventional quantum theory and Maxwell theory and thus the validity of the EEP. All units, but the Kelvin, are thus influenced by relativity. – Consequently, OPTIS may be considered as a metrology mission.

Table I. The scientific objectives of the OPTIS mission: present status and planned accuracy. *Accuracies are given in terms of Mansouri–Sexl parameters (see below), **The authors of [12] claims a different, more pessimistic error budget. See also [13, 14], ***Using a newly developed method for analyzing LAGEOS satellites data, the present accuracy for testing the Newtonian potential will increase to 10^{-11} [15]. However, the influence of certain tiny non-gravitational perturbations of thermal origin has not been considered in that study. See also [16].

	test	method	present accuracy	OPTIS accuracy
1	isotropy of speed of light*	cavity–cavity comparison	$1.5 \cdot 10^{-9}$ [2]	10^{-12}
2	constancy of speed of light *	cavity–clock comparison	$7 \cdot 10^{-7}$ [3]	10^{-8}
3	time dilation – Doppler effect	laser link	$2 \cdot 10^{-7}$ [4]	10^{-9}
4	universality of gravit. redshift I	cavity–clock comparison	$1.7 \cdot 10^{-2}$ [5]	10^{-4}
5	universality of gravit. redshift II	clock–clock comparison	$2.5 \cdot 10^{-5}$ [6]	10^{-7}
6	absolute gravitational redshift	time transfer	$1.4 \cdot 10^{-4}$ [7]	10^{-8}
7	Lense-Thirring effect**	laser tracking	0.3 [8]	10^{-3} [9]
8	Einstein perigee advance	laser tracking	$3 \cdot 10^{-3}$ [10]	$6 \cdot 10^{-4}$ [9]
9	test of Newton potential***	laser tracking	10^{-5} [11]	10^{-12} [9]

A11

For GR, we have the Universality of Free Fall (UFF, also called Weak Equivalence Principle), the Universality of the Gravitational Redshift (UGR, also called Local Position Invariance), and the fact that the local nongravitational experiments carried out in frames with different orientation and velocity are described by SR (also called Local Lorentz Invariance). These three principles form the Einstein Equivalence Principle (EEP) from which one argue that gravity must be described by a metric theory, that is, within the mathematical frame of the pseudo-Riemannian geometry. Tests of two of these three principles are part of the OPTIS science goals.

Einstein's field equations, and thus GR, cannot be deduced from the EEP alone. This task can in part be accomplished, at the weak field and slow motion order, within the framework of the Parametrized Post–Newtonian (PPN) formalism which introduces very general relations between the sources of the gravitations field and the structure of the space-time metric. All standard tests and all observations of gravitationally induced effects, like solar system tests or observations of binary pulsars, can be used for that purpose. The measurements of the Lense–Thirring effect, of the absolute gravitational redshift, and the verification of the Newtonian $1/r$-potential are among these tests.

2. BASIC SCIENCE GOALS

As motivated in the previous section, the scientific objectives of the OPTIS mission (compare Table II) are the improvement of the

1. test of the isotropy of light propagation by three orders of magnitude,

Table II. Science relevant orbit data. The heights of apogee and perigee are given relative to the Earth's surface.

	apogee	perigee
height	36238 km	10000 km
velocity	4.33 km/s	6.99 km/s
gravitational potential/c^2	$1.0 \cdot 10^{-10}$	$2.7 \cdot 10^{-10}$
gravity gradient	$5.2 \cdot 10^{-9}$ s^{-2}	$9.1 \cdot 10^{-8}$ s^{-2}

2. tests of the independence of the velocity of light from the velocity of the laboratory by two orders of magnitude,
3. test of the special relativistic time–dilation by one order of magnitude,
4. test of UGR by comparison of optical clocks based on resonators and atomic clocks by two orders of magnitude,
5. test of UGR by comparison of two atomic clocks by two orders of magnitude,
6. measurement of the absolute gravitational redshift by 2 orders of magnitude (this will include the first measurement of the second–order redshift),
7. measurement of the gravitomagnetic Lense-Thirring effect by two orders of magnitude,
8. measurement of the gravitoelectric Einstein perigee advance and thus of the PPN parameters γ and β by one order of magnitude, and
9. test of Newton's $1/r$ gravitational potential by one order of magnitude.

Except for the UFF, which will be tested by MICROSCOPE and STEP, OPTIS represents a complete test of the foundations of the metric theories of gravity, see Fig. 3. Furthermore, relativistic orbital effects as predicted by Einstein's theory of gravity, will be tested.

3. MISSION SCENARIO

The mission scenario is shown in Fig. 5. The satellite is in a highly elliptical orbit, see Table II. Characteristic properties of the orbit are given in Table III. One important point is the long five-month period without any shadow phase that allows stable thermal conditions inside the satellite.

The satellite spins around its symmetry axis which points toward the sun in order to avoid heavy changes in the thermal environment. The spinning rate can be varied between 10^{-2} and 10^{-4} Hz. While orbiting the Earth, the experiments testing the isotropy and constancy of the velocity of light, as well as the various

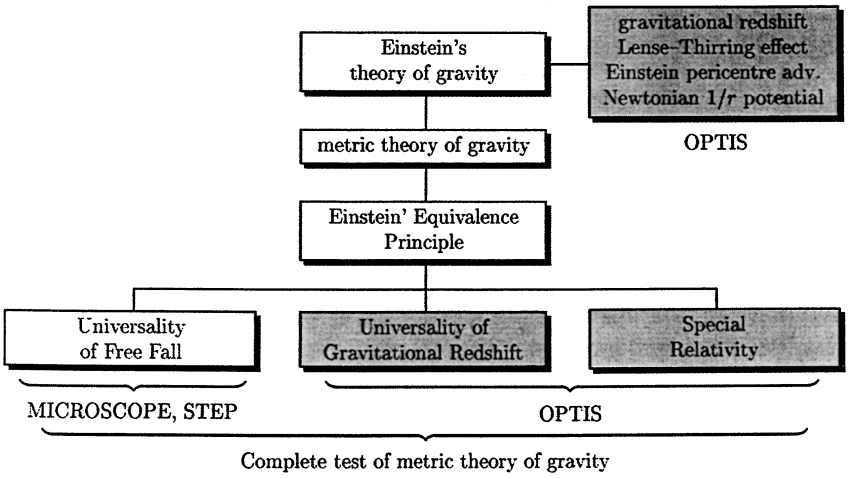

Figure 3. Together with MICROSCOPE or STEP, OPTIS will provide a full test of the metric structure of the gravitational field. Furthermore, effects characteristic of the Einstein field equations, namely the Lense–Thirring effect, the Einstein pericentre advance and the validity of the Newtonian $1/r$ potential, will be tested by OPTIS.

redshift experiments, are carried through. At the same time, laser tracking will yield high precision orbit data.

OPTIS is a mission which uses technologies which have already been demonstrated, and combines them in such a way that a wealth of science goals can be achieved. For example, high performance of the SR experiments requires a drag-free motion in order to avoid deformations of the resonators due to external forces. This drag-free attitude control is also used for the satellite to follow very precisely the geodesic path around the Earth. In addition to orbit and attitude control, the satellite may also be tracked by laser ranging thus giving further high precision orbit information. Here, tracking is passive and is independent from the scientific payload designed for the isotropy and constancy of the speed of light and clock tests. Due to this multi–use of applied techniques, OPTIS is a very efficient science mission.

Table III. Orbit characteristics.

period	14 h
inclination	63.43°
solar radiation	radiation pressure = 4.4 μN/m^2
Earth albedo	radiation pressure = 1.2 μN/m^2
shadow	5 months without shadow, 1 month with shadow phases

4. THEORETICAL DESCRIPTION OF EXPERIMENTS

All planned tests are in fact comparisons of rates of clocks of various kinds:

- In tests of the isotropy of the velocity of light the frequencies defined by resonators ("light clocks") pointing in different orientations are compared,
- in tests of the constancy of the velocity of light a resonator clocks and atomic clocks under the conditions of varying velocities are compared,
- in tests of the time dilation (or Doppler) effect the rates of clocks in different states of motion are compared,
- in tests of the UGR one compares clocks moving together through a non–constant gravitational potential, and, finally,
- in measurement of the gravitational redshift one compares clocks at different positions in the gravitational field, see Fig. 4.

The other tests are derived from tracking the satellite in its very precise geodesic orbit. These observation allow to derive conclusions about the effects of the gravitational field of the Earth, like the Einstein gravitoelectric perigee advance, and the gravitomagnetic Lense-Thirring effect due to the Earth's rotation, and estimates on hypothetical Yukawa parts of the Newtonian potential.

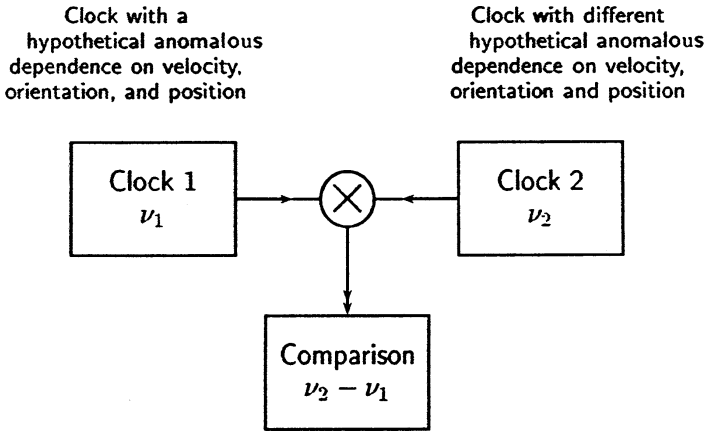

Figure 4. General scheme for testing SR and GR with clocks. Tests of the constancy of the speed of light and of UGR are essentially carried through with clocks whose frequency may change with orientation, velocity, and position. If furthermore, the clocks are assumed to move with different velocities or to be at different positions, then this scheme also applies to tests of the time dilation and of the gravitational redshift.

4.1. SR Experiments

SR has two aspects: First, it describes the transformation between various inertial systems, and second, it is related to the velocity of light which is a consequence of dynamical equations, namely the Maxwell equations. Consequently, tests of SR can be described on two levels, either kinematically or dynamically.

4.1.1. Kinematical Description

Kinematical test theories start from a preferred frame (with coordinates T and $\boldsymbol{X}$) which usually is identified with the frame in which the cosmic microwave background is isotropic (bold-face symbols denote 3–vectors). In this frame light is assumed to propagate isotropic[7] with velocity c_0, that is $\boldsymbol{X}^2 = c_0^2 T^2$ (in the following we set $c_0 = 1$). Moving frames (with coordinates t and $\boldsymbol{x}$) are defined by the requirement that a force–free motion appears rectilinear and uniform. Different frames with this property are related by projective transformations. The further requirement that these transformations are one-to-one leads to linear transformations. The most general ansatz for the coefficients of this linear transformation in terms of the velocity $\boldsymbol{v}$ between two frames leads to (see, e.g., [17])

$$T = \frac{1}{a(v)}\,(t - \boldsymbol{\epsilon}\cdot\boldsymbol{x}) \tag{1}$$

$$\boldsymbol{X} = \frac{1}{d(v)}\boldsymbol{x} - \left(\frac{1}{d(v)} - \frac{1}{b(v)}\right)\frac{\boldsymbol{v}(\boldsymbol{v}\cdot\boldsymbol{x})}{v^2} - \frac{1}{a(v)}\boldsymbol{v}(\boldsymbol{\epsilon}\cdot\boldsymbol{x}) + \frac{1}{a(v)}\boldsymbol{v}t\,, \tag{2}$$

where a, b, and d are unknown functions of the velocity and $\boldsymbol{\epsilon}$ describes the synchronization in the frame under consideration. The two-way velocity of light c turns out to be independent of the synchronization

$$c(\vartheta, v) = \frac{d\sqrt{1-v^2}}{a}\,\frac{1}{\sqrt{1 + A\cos^2\vartheta}}\,, \tag{3}$$

where we defined the anisotropy

$$A(v) = \frac{d^2(v)}{b^2(v)(1-v^2)} - 1\,, \tag{4}$$

[7] This is a requirement which needs additional input. Kinematical test theories are not complete. In other words, the required existence and identification of the preferred frame is part of the test theory. If our knowledge about the universe changes by, e.g., identifying another preferred frame (perhaps singled out by properties of gravitational radiation), we then have a different test theory and all the interpretations within this test theory will also change. Therefore, dynamical test theories (see below) which do not need such an extra input, are complete and are, thus, favoured.

and where ϑ is the angle between the velocity $\boldsymbol{v}$ and the direction of light propagation. For $v \ll 1$ we can expand the coefficient functions to order v^2 [18–20]

$$a(v) = 1 + \left(\alpha - \frac{1}{2}\right) v^2 + \mathcal{O}(v^4)\,, \tag{5}$$

$$b(v) = 1 + \left(\beta + \frac{1}{2}\right) v^2 + \mathcal{O}(v^4)\,, \tag{6}$$

$$d(v) = 1 + \delta v^2 + \mathcal{O}(v^4) \tag{7}$$

and get for the two-way velocity of light

$$c(\vartheta, v) = 1 + \left[\beta - \alpha + (\beta - \delta)\cos^2\vartheta\right] v^2\,. \tag{8}$$

Note that our definition of the coefficients α, β and δ is different from [18].

The frequency of a standing wave in a resonator can be derived from the plane wave ansatz $\varphi = Ae^{-i(\omega t - k_+ x)} + Be^{-i(\omega t - k_- x)}$ where $\pm$ corresponds to the propagating/counterpropagating wave (due to the stationarity of the problem, both waves must possess the same frequency). We use the general dispersion relation $\omega = c_\pm k_\pm$ where the velocity of light depends on the direction and the velocity of the frame, $c_\pm = c_\pm(\vartheta, v)$, and the boundary condition $\varphi(0) = \varphi(L) = 0$ and get the condition

$$\nu(\vartheta, v) = \frac{n}{2L} c(\vartheta, v)\,, \tag{9}$$

for the frequency $\nu = \omega/2\pi$ where $c(\vartheta, v)$ is the two-way velocity of light defined by $2/c = 1/c_+ + 1/c_-$. If the two-way velocity of light depends on the orientation of the resonator or on the state of motion of the laboratory, then a change in the orientation or the velocity of the laboratory results in a change of the frequency.

The comparison of the frequencies of two resonators oriented orthogonally gives the frequency difference[8]

$$\nu(\vartheta + \tfrac{\pi}{2}, v) - \nu(\vartheta, v) = \frac{n}{2L}\left(c\left(\vartheta + \frac{\pi}{2}, v\right) - c(\vartheta, v)\right). \tag{10}$$

The isotropy of the speed of light, that is, its invariance under changes of the orientation ϑ, can be tested by comparison of the frequency (9) with an independent frequency, or by measuring the frequency difference (10). As a result we get $A = 0$, that is, $d = b\sqrt{1 - v^2}$. In the linearized form we get $\beta = \delta$. The presently best estimate is $|\beta - \delta| \leq 4 \cdot 10^{-9}$ [2]. With OPTIS this may be improved by three orders.

[8] Experiments of this type are usually called Michelson–Morley experiments where interferometric methods are used. The comparison of the frequency of two cavities can also be regarded as an interferometric experiment.

A change in the velocity of the whole apparatus consisting of cavities and lasers etc., can be used for a test of the constancy of the speed of light, that is, its independence on the velocity of the laboratory. For this, we have to use (9) and compare this with an independent frequency standard because in the case of isotropy (10) would give a null result[9]. Assuming isotropy, the constancy of the frequency gives $d\sqrt{1-v^2}/a = 1$, or $a/b = 1 - v^2$. In the linearized form we get $\alpha = \beta$. The presently best test gives $|\alpha - \beta| \leq 7 \cdot 10^{-7}$ [3] and may be improved by OPTIS by two orders of magnitude.

At last, time–dilation experiments can determine the yet unknown function $a(v)$. This kind of experiments compare the rate of two identical clocks (with rates ν_0 in their rest frame) moving with velocities differing by the relative velocity $\boldsymbol{v}$. For simplicty, we assume one clock (the sender) to be at rest, and the other (the receiver, which carries the other clock) moving with v in radial direction. The sender emits a signal with frequency ν_0 (in its rest frame) which will be received by the receiver with frequency ν'. This frequency will be sent back so that the sender measures a frequency ν''. Simultaneously, the receiver also emits a signal with the frequency ν_0 defined by its own clock which will be observed by the sender with frequency ν'. From these frequencies we first have to define the two–way Doppler signal $D = (\nu'' - \nu_0)/\nu_0$ and the redshift signal $R = (\nu' - \nu_0)/\nu_0 - D/2$ [21]. These quantities do not depend on any synchronization.

One can now introduce a (synchronization independent) velocity V by means of $D = -2V/(1 - V)$ which, in the case of Einstein synchronization, coincides with the measured velocity. Thus, with D one can determine the velocity of the receiver in a synchronization–independent way. This can be used to express R as a function of the velocity V and the velocity with respect to the preferred frame (see [21] for the rather involved calculations), or to express R as a particular function of D. Within SR, this function has a specific form, namely $R = \sqrt{D+1} - \frac{D}{2} - 1$. The confirmation of this function amounts to fixing $a = \sqrt{1-v^2}$. For a parametrization of a deviation from this SR form, $a = \sqrt{1-v^2} + \frac{1}{2}\alpha v^2$, recent experiments [4] give $\alpha \leq 2 \cdot 10^{-7}$. With the mission GP-A this effect has been confirmed to the order 10^{-6}. With clocks reaching an instability of 10^{-16}, a laser link which reaches the same instability, and a sampling of a few thousand orbits, OPTIS may reach a result with an accuracy of up to 10^{-9}.

However, the method of using an independent frequency standard needs a remark of caution: The independent frequency standard is given by an atomic or molecular transition. In general, this transition may depend on the velocity of

[9] The first experiments testing the constancy of the speed of light has been carried through by Kennedy and Thorndike who used an interferometer with unequal arm length. Experiments of this kind are called Kennedy–Thorndike experiments. In the experiments considered here a resonator is compared with an atomic or molecular frequency standard which is assumed not to depend on the velocity.

the laboratory, too. However, the atomic or molecular spectra depend on other physical laws than the velocity of light: while the velocity of light depends on the Maxwell equations only, the atomic spectra also depend on the properties of quantum matter which, in general, may also reveal violations of SR (which are tested by Hughes–Drever experiments). Therefore, a comparison of different frequency standards basically explores whether different fundamental physical laws (like Dirac and Maxwell equations) behave similarly, thus amounting to a test of the relativity principle.

4.1.2. Dynamical Description

For the description of the tests by means of a dynamical test theory we have to replace all the dynamical equations governing the behaviour of all physical systems participating in these experiments by generalized equations of motions which lead to violations of SR. Since nuclear forces are significant on a small scale or at high energies only, a good ansatz for a dynamical description of these tests consists of a modification of the Maxwell and of the Dirac equation for electrons and protons. A modified Maxwell equation results in a modification of the properties of light and of the electric and magnetic field of e.g. pointlike sources. A modified Dirac equation will result in a modification of atomic spectra and a modification of the behaviour of solids, e.g. cavities. Only all modifications together will determine the outcome of experiments. Thus it might happen, at least in principle, that two SR–violating parts cancel out each other. This has to be calculated in each case. Furthermore, it also has to be explored how many experiments are needed in order to derive SR within this dynamical scheme (in the case of the kinematical test theories three tests are sufficient).

One example of a dynamical test theory for SR is the c^2-formalism which is the coordinate independent version of the $TH\epsilon\mu$-formalism [22–24]. In this test theory (which is designed in order to emphasize the hypothetical possibility of different limiting velocities for matter and for light) only one parameter has to be determined. Thus, with one experiment one can derive SR. A much more complete test theory is given by the formalism of Ni [25, 26] who first related some generalized Maxwell equations to astrophysical observations and also showed that modified Maxwell equations in general lead to violation of the Universality of Free Fall. Furthermore, [27] as well as [28] used generalized Maxwell equations for the interpretation of astrophysical data. Later Kostelecky and co-workers [29, 30] used that formalism to describe laboratory tests as well as astrophysical observations. Another test theory is outlined in [31].

Dynamical test theories became important because modified Maxwell equations as well as modified Dirac equations were derived in the low energy limit from string theory as well as from loop gravity [32–39].

The Ni–Haugan–Kostelecky Formalism. The starting point in the dynamical test theory describing a wide range of possible Lorentz violation schemes is the $\chi - g$ test theory of of Ni [25, 26, 40, 41] which has also been used by Haugan and Kauffmann [28], together with the extension to the Dirac sector employed by Kostelecky and co-workers [29, 30, 42, 43] which, altogether, is called the Standard Model Extension. It is given by the Lagrangian

$$\mathcal{L} = \frac{1}{16\pi}(\eta^{ac}\eta^{bd} + \lambda^{abcd})F_{ab}F_{cd} + \frac{i}{2}\bar{\psi}\Gamma^a \overleftrightarrow{D}_a \psi - \bar{\psi}M\psi \tag{11}$$

with the gauge covariant derivative $D_a = \partial_a - ieA_a$ where A_a is the electromagnetic potential and the Minkowski metrics $\eta^{ab} = \mathrm{diag}(1, -1, -1, -1)$ $(a, b, c, \ldots = 0, \ldots, 3)$. The electromagnetic field strength is $F_{ab} = \partial_a A_b - \partial_b A_a$. The first part is the Maxwell sector, the second part the fermion sector of the theory. The tensor λ^{abcd} possesses 19 independent coefficients. From the form of Lagrangian the tensor λ^{abcd} possess the symmetries

$$\lambda^{abcd} = \lambda^{ab[cd]} = \lambda^{[ab]cd} = \lambda^{cdab}, \qquad \lambda^{a[bcd]} = 0. \tag{12}$$

Furthermore, the double trace can be absorbed into a re-definition of the unit charge. Therefore, λ^{abcd} possesses effectively 19 independent degrees of freedom.

The Maxwell Sector. The equations of motion for the electromagnetic field are given by

$$(\eta^{ac}\eta^{bd} + \lambda^{abcd})\partial_b F_{cd} = 4\pi j^a\,. \tag{13}$$

In $3 + 1$-form, these equations read

$$\nabla \cdot \boldsymbol{D} = 4\pi\rho \qquad \nabla \times \boldsymbol{H} = \dot{\boldsymbol{D}} + 4\pi\,\boldsymbol{j} \tag{14}$$

$$\nabla \cdot \boldsymbol{B} = 0 \qquad \nabla \times \boldsymbol{E} = -\dot{\boldsymbol{B}} \tag{15}$$

with

$$\boldsymbol{D} = \boldsymbol{E} + \kappa_{DE}\boldsymbol{E} + \kappa_{DB}\boldsymbol{B} \tag{16}$$

$$\boldsymbol{H} = \boldsymbol{B} + \kappa_{HB}\boldsymbol{B} + \kappa_{HE}\boldsymbol{E} \tag{17}$$

where the κ's are 3×3-matrices depend on λ^{abcd}

$$(\kappa_{DE})^{ij} = 2\lambda^{i0j0}, \qquad (\kappa_{DB})^{ij} = \lambda^{0ikl}\epsilon_{jkl} \tag{18}$$

$$(\kappa_{HB})^{ij} = \frac{1}{2}\epsilon_{ikl}\lambda^{klmn}\epsilon_{jmn}, \qquad (\kappa_{HE})^{ij} = -\epsilon_{ikl}\lambda^{kl0j} \tag{19}$$

$(i, j, k, \ldots = 1, 2, 3)$. They possess the symmetries

$$\kappa_{DE}^T = \kappa_{DE}, \quad \kappa_{HB}^T = \kappa_{HB}, \quad \kappa_{DB} = -\kappa_{HE}^T,$$
$$\mathrm{tr}\kappa_{DB} = 0, \quad \mathrm{tr}(\kappa_{DE} + \kappa_{HB}) = 0. \tag{20}$$

The two dynamical equations which govern the propagation of light rays, are, in terms of E_i and B_i

$$0 = \dot{\boldsymbol{E}} + \kappa_{DE}\dot{\boldsymbol{E}} + \kappa_{DB}\dot{\boldsymbol{B}} - \boldsymbol{\nabla} \times (\boldsymbol{B} + \kappa_{HB}\boldsymbol{B} + \kappa_{HE}\boldsymbol{E}) \tag{21}$$

$$0 = \dot{\boldsymbol{B}} + \boldsymbol{\nabla} \times \boldsymbol{E}\,, \tag{22}$$

or as equations for 6-components vectors

$$\begin{aligned} 0 \;&= \begin{pmatrix} \delta_{ik} + (\kappa_{DE})_{ij} & (\kappa_{DB})_{ij} \\ 0 & \delta_{ik} \end{pmatrix} \frac{d}{dt} \begin{pmatrix} E_k \\ B_k \end{pmatrix} \\ &\quad + \begin{pmatrix} -\epsilon_{ijk}(\kappa_{HE})_{kl} & -\epsilon_{ijl} - \epsilon_{ijk}(\kappa_{HB})_{kl} \\ \epsilon_{ijl} & 0 \end{pmatrix} \partial_j \begin{pmatrix} E_l \\ B_l \end{pmatrix}. \end{aligned} \tag{23}$$

Making the ansatz for plane waves, $\boldsymbol{E} = \boldsymbol{E}^0 e^{-i(\omega t - \boldsymbol{k}\cdot\boldsymbol{x})}$, $\boldsymbol{B} = \boldsymbol{B}^0 e^{-i(\omega t - \boldsymbol{k}\cdot\boldsymbol{x})}$, gives a linear system for $(\boldsymbol{E}, \boldsymbol{B})$. The requirement of a nonzero solution is the vanishing of the determinant, which results in a dispersion relation possessing, in general, 6 solutions. Without the anomalous terms, the determinant reads $\omega^2(\omega^2 - \boldsymbol{k}^2)^2$ with two solutions $\omega = 0$ and four solutions $\omega = \pm|\boldsymbol{k}|$. Since we are interested in the future–pointing propagating modes, we look for solutions $\omega = |\boldsymbol{k}| + \delta\omega$ for small $\delta\omega$. Making an expansion to second order in $\delta\omega$ and keeping only terms first order in the anomalous parameters, we get as frequency

$$\omega = \left(1 + \rho(n) \pm \sqrt{\sigma^2(n) - \rho^2(n)}\right) |\boldsymbol{k}| \tag{24}$$

with

$$\rho(n) = -\frac{1}{2}\eta_{ac}\chi^{abcd}n_b n_d \tag{25}$$

$$\sigma^2(n) = \frac{1}{2}\eta_{ae}\eta_{cg}\chi^{abcd}\chi^{efgh}n_b n_d n_f n_h \tag{26}$$

where $n_a = k_a/|\boldsymbol{k}| \approx (1, k_i/|\boldsymbol{k}|)$ denotes the direction of the light's momentum. Note that ρ and σ are scalars, that is, they do not depend on the frame.

From this result it is obvious that in general light shows birefringence and propagates with different velocity in different directions. This formalism has been used [30] to describe astrophysical searches for birefringence and experiments with microwave and optical resonators.

No birefringence occurs if and only if $\sigma^2(n) - \rho^2(n) = 0$ for all n_a. This implies

$$\begin{aligned} 0 &= \frac{1}{2}\eta_{ae}\eta_{cg}\chi^{abcd}\chi^{efgh}n_b n_d n_f n_h - \frac{1}{4}\eta_{ac}\chi^{abcd}n_c n_d \eta_{eg}\chi^{efgh}n_f n_h \\ &= \frac{1}{2}\left(\eta_{ae}\eta_{cg}\chi^{abcd}\chi^{efgh} - \frac{1}{2}\eta_{ac}\chi^{abcd}\eta_{eg}\chi^{efgh}\right) n_b n_d n_f n_h\,. \end{aligned} \tag{27}$$

This is a relation of the structure $A^{abcd}n_an_bn_cn_d = 0$ for all n_a obeying $\eta^{ab}n_an_b = 0 + \mathcal{O}(\chi)$. In n_a the corrections of order χ can be neglected. As a result, we get $A^{(abcd)} = \eta^{(ab}\mu^{cd)}$:

$$\underset{bdfh}{S}\left(\eta_{ae}\eta_{cg}\chi^{abcd}\chi^{efgh} - \frac{1}{2}\eta_{ac}\chi^{abcd}\eta_{eg}\chi^{efgh}\right) = \eta^{(bd}\mu^{fh)}, \tag{28}$$

where $\underset{bdfh}{S}$ denotes total symmetrization in the indicated indices. Consequently, the coefficients χ^{abcd} are reduced to 11 independent quantities, 10 encoded in the symmetric tensor μ^{ab} and one pseudoscalar (compare [44]):

$$\chi^{abcd} = \eta^{a[c}\mu^{d]b} + \chi\epsilon^{abcd}, \tag{29}$$

where χ is a pseudoscalar and ϵ^{abcd} the totally antisymmetric Levi–Civita tensor. In terms of the κ's this gives

$$(\kappa_{DE})^{ij} = \mu^{ij}\,, \qquad (\kappa_{DB})^{ij} = 2\chi\delta^{ij} \tag{30}$$

$$(\kappa_{HB})^{ij} = \frac{1}{2}(\mu^{ij} - \delta^{ij}\mathrm{tr}\mu), \qquad (\kappa_{HE})^{ij} = 2\chi\delta^{ij}. \tag{31}$$

It has been shown in [30] that the combinations $\kappa_{DE} + \kappa_{HB}$ and $\kappa_{DB} - \kappa_{HE}$ are tightly constrained by astrophysical observations: they are smaller than $4 \cdot 10^{-32}$. Nine other coefficients enter the relation describing the frequency shift in resonators [30]

$$\frac{\delta\nu}{\nu} = -\frac{1}{2}\left(\hat{E}^*\kappa_{DE}\hat{E} - (\hat{n}\times\hat{E}^*)\kappa_{HB}(\hat{n}\times\hat{E})\right)\,, \tag{32}$$

where $\hat{n}$ is the direction of the cavity and $\hat{E} = \vec{E}/|\vec{E}|$. It has been shown in [45] that the modifications of the geometry of the resonator due to the modifications of the Maxwell equations are two orders smaller than the effects due to the modifications in the properties of light propagation and, thus, can be neglected here. Since the κ_{DE} and κ_{HB} are second-rank tensors, a rotation of the resonator around an arbitrary axis by the angle ϑ results in a directional behaviour of the frequency shift according to

$$\frac{\delta\nu(\vartheta)}{\nu} = A + B\sin(2\vartheta) + C\cos(2\vartheta)\,, \tag{33}$$

where the coefficients A, B, and C depend on the Lorentz violation parameters in the actual frame. From recent experiments [2], the coefficients κ_{DE} and κ_{HB} can be estimated to be smaller than 10^{-14}. OPTIS again aims at an improvement by three orders of magnitude.

The Dirac Sector. In general, it is possible that Lorentz–violating terms might enter the equations of motion in any of the (photon, electron, . . .) sectors of the standard model. They can be described by a generalized Lagrangian Eq. (11),

for example by letting $\Gamma_a = \gamma_a + c_{ba}\gamma^b + \tilde{\Gamma}_a$, where γ_a are the conventional Dirac matrices and c_{ab} is a tensor in which Lorentz violation is encoded. This form of the Lagrangian is of particular interest, as it arises in non-commutative geometry as a consequence of string theory under very general assumptions [37]. The matrix $\tilde{\Gamma}_a$ denotes other possible Lorentz–violating terms [42, 43, 46]. In a non–relativistic approximation, this leads to a modified Pauli equation

$$H\psi = \left(\frac{p^2}{2m} + E^{ij}\frac{p_i p_j}{m} + F^{ij}{}_k\frac{p_i p_j}{m}\sigma^k + C^i p_i + D^i_j p_i \sigma^j + mA + mB_i\sigma^i\right)\psi, \tag{34}$$

where the coefficients $A, \ldots, F$ depend on Lorentz–violating parameters where, and this is important for the experiments described below, $E^{ij} = -c^{ij} - \frac{1}{2}c^{00}\delta^{ij}$ depends on c_{ab} only. Stringent bounds on many of them exist from atomic clock–comparison experiments [47]. Performing such experiments in space leads to greatly improved sensitivity, as discussed in [48]. This offers several attractive options for comparisons between the clocks on board the OPTIS satellite.

Experiments of this type are, unfortunately, not sensitive to the tensor c_{ab}. However, it has been shown recently [49] that c_{ab} can be measured in frequency comparisons using cavities. It leads to a modified kinetic energy term for electrons; since the electrons within a solid have a non–zero kinetic energy which depends on the crystal geometry, a non-zero c_{ab} induces a change of the geometry of the crystal. Thus, the dimensions of a cavity made from this crystal will change due to c_{ab}. Therefore, the change in the geometry, which usually is expressed in terms of the strain tensor S_{ij} (see Sec. 5.5.2), can be related to Lorentz–violating quantity E_{ij} by [49]

$$S_{ij} = B_{ijkl}E_{kl}\,, \tag{35}$$

where B_{ijkl} is a dimensionless "sensitivity tensor". It can be shown that it depends on material parameters such as the primitive lattice vectors and the elastic moduli of the material and, thus, can be calculated. The resonance frequency ν of a cavity pointing in x^1 direction, for example, will thus be shifted by $\delta\nu/\nu = -\delta L/L = -B_{11kl}E_{kl}$, or $\delta\nu/\nu = -B_{1111}E_{11} - B_{1122}(E_{22} + E_{33})$ for isotropic materials. The dependence of B_{ijkl} on the cavity material allows it to separate the signal from the signal for Lorentz violation in electrodynamics, by comparing cavities made from different materials or two similar cavities pointing in different directions and atomic clocks. This leads to independent limits on both effects.

This offers the possibility of measuring c_{ij} by using cavities. The only limits presently known are [49] $|c_{XX} + c_{YY} - 2c_{ZZ}| \lesssim 10^{-12}$, $|c_{(XY)}| \lesssim 8 \times 10^{-15}$, and $|c_{XX} - c_{YY}| \lesssim 1.6 \times 10^{-14}$. They have been derived by this method from a reanalysis of terrestrial isotropy experiments. These involved a quartz cavity, for which the elements of the sensitivity tensor are generally a factor of about three smaller compared to the corresponding values for silicon, which is projected for OPTIS.

A 1000 fold improvement of the isotropy experiment by OPTIS will thus give a 3000 fold improved limit on c_{ij} at a level of 10^{-18}. The orbital motion of the satellite also offers the possibility of restricting all but one degree of freedom in the symmetric part of c_{ij}. In the framework of non-commutative geometry [37], the improved bound on c_{ij} will lead to the best upper limit on the non-commutation parameters.

Generalized Maxwell Equations. The Maxwell sector can be further generalized for a test theory which, among others, is also capable to describe tests of charge conservation [31,50]. One starts with the most general first order linear system for the field strength

$$(\eta^{ac}\eta^{bd} + \chi^{abcd})\partial_b F_{cd} + \chi^{acd} F_{cd} = 4\pi j^a \,. \tag{36}$$

In contrast to (13), the tensor χ^{abcd} has only the symmetry $\chi^{abcd} = \chi^{ab[cd]}$ and, thus, possesses 92 independent coefficients ($4 \times 4 \times 6$ from the antisymmetry in the last two coefficients, minus 4 due to the homogeneous Maxwell equations $\partial_{[a} F_{bc]} = 0$). The term χ^{acd} [31] has the properties of an anisotropic photon mass. Even in the special case $\chi^{abcd} = 0$ and $\chi^{acd} = \eta^{ac}\theta_b$, the group and phase velocities of light will depend on the direction of propagation and also on the frequency, i.e., they show dispersion. This makes this term observable in Michelson–Morley–like interferometry or cavity experiments. A modification of the Coulomb potential leading to a direction–dependent Yukawa potential will also occur. It will affect the length of interferometer arms (made, for example, out of ionic crystals) and can thus lead to a cancellation of effects [31]. However, for the commonly used microwave or optical frequencies, the cancellation part is too small to be of any experimental importance. Therefore, also in this case the commonly used interpretation of these experiments is still valid.

In addition to the effects related to Eq.(13), the reduced symmetry of the tensor χ^{abcd} allows the description of charge non-conservation. Charge non-conservation is related to the part $\chi^{(ab)cd}$ that is symmetric in the first index pair, according to $\partial_a j^a \sim \chi^{abcd}\partial_a\partial_b F_{cd}$. Also these components lead to an anisotropic speed of light [51]. Consequently, isotropy experiments also serve as a test of charge conservation. Since the isotropy of the speed of light has been confirmed within 10^{-14} accuracy [45] in the coefficients χ^{abcd}, this gives a corresponding limit on charge non-conservation[10]. Again, OPTIS will also improve this test by three orders of magnitude. It should be stressed that while a (hypothetical) time-dependence of the fine structure constant not necessarily has to be interpreted as a time–dependent

[10] It is interesting to note that in the case of constant c and $\hbar$, the conservation of the electron charge as derived from the estimate of the time-dependence of the fine structure constant $\dot{\alpha}/\alpha \leq 10^{-15}$ y^{-1} [52] is of approximately the same order.

electric charge, the outcome of isotropy experiments necessarily gives a constraint on charge conservation.

4.2. GR Experiments

4.2.1. The Gravitational Redshift

Within a metric theory of gravity, the gravitational redshift experienced by identical clocks placed at different stationary positions in stationary gravitational fields is given in coordinates adapted to the symmetry by the zero components of the space-time metric

$$\frac{\nu(x_2)}{\nu(x_2)} = \frac{\sqrt{g_{00}(x_2)}}{\sqrt{g_{00}(x_1)}}. \tag{37}$$

In a post–Newtonian approximation this is

$$\frac{\nu(x_2)}{\nu(x_1)} = 1 - \frac{U(x_2) - U(x_1)}{c^2}, \tag{38}$$

where $U(x)$ is the Newtonian potential. The most precise measurement of this redshift has been carried out by the GP-A mission in 1978 [7]. The prediction (38) has been verified to $1.4 \cdot 10^{-4}$ precision with H-masers onboard a rocket and on ground using a transponder technique. For the OPTIS orbit frequency shifts between $(\nu_{\text{apogee}} - \nu_{\text{ground}})/\nu_{\text{ground}} = 5.9 \cdot 10^{-10}$ and $(\nu_{\text{perigee}} - \nu_{\text{ground}})/\nu_{\text{ground}} = 4.2 \cdot 10^{-10}$ are calculated. With today's clock stability approaching $1 \cdot 10^{-16}$ the redshift would become measurable with an accuracy of $\delta\nu/\nu \approx 10^{-6}$. In addition, the large number of orbits (1000 orbits are slightly more than a year) further increases the accuracy towards the order 10^{-8}.

Within a PPN framework, all terms up to the order $1/c^4$ including the quadrupole moment and the angular momentum of the rotating Earth [53] have been calculated. This result shows that for the interpretation of OPTIS measurements it is necessary to take into account mass monopole terms up to the order $1/c^4$ and relativistic quadrupole order terms: The $1/c^3$ order mass monopole term leads to a frequency shift of $\sim 2 \cdot 10^{-14}$, the $1/c^4$ mass monopole term to a shift of the order 10^{-18}. The relativistic quadrupole term gives a shift 10^{-16} (the non-relativistic multipole contributions are of course included in (38)). The rotation of the Earth affects clocks only at the 10^{-19} level. Also the second order PPN contribution U^2/c^4 is of the order $5 \cdot 10^{-19}$.

4.2.2. The Universality of the Gravitational Redshift

If the gravitational redshift is not universal, the frequencies of the various types of clocks at the different positions in the gravitational field will depend on

the *type* of the clock. Thus (38) has to be modified to

$$\nu(x_1) = \left(1 - (1 + \alpha_{\text{clock}})\frac{U(x_1) - U(x_0)}{c^2}\right)\nu(x_0)\,. \tag{39}$$

In GR, $\alpha_{\text{clock}} = 0$ for all clocks, such as atomic clocks, optical resonators, H–maser, quartz crystals, etc. In terms of α_{clock} the Vessot–Levine experiment yielded $|\alpha_{\text{clock}}| \leq 1.4 \cdot 10^{-4}$. OPTIS aims at a test of this gravitational redshift with up to three orders of improvement, that is up to $|\alpha_{\text{clock}}| \leq 10^{-7}$. In comparison, the planned experiments ACES-PHARO, SUMO, and PARCS to be carried through onboard of the ISS [54] are supposed to reach the 10^{-5} level, while the ISS project RACE is projected to approach the 10^{-7} level. As compared to the ISS, OPTIS has the advantage to fly on a high elliptic orbit, to have a long mission time and to have various clocks onboard (optical resonators, ion clocks, etc.).

If the redshift depends on the type of clock, then the clocks exhibit different redshifts. Moving both clocks together in the gravitational field (as will be done in the OPTIS mission with an atomic clock and an optical resonator, see Fig. 5), gives for the ratio of the frequencies of these two clocks

$$\frac{\nu_1(x_1)}{\nu_2(x_1)} \approx \left(1 - (\alpha_{\text{clock2}} - \alpha_{\text{clock1}})\frac{U(x_1) - U(x_0)}{c^2}\right)\frac{\nu_1(x_0)}{\nu_2(x_0)}\,. \tag{40}$$

In case of a violation of the UGR we get a *position dependent* frequency ratio which is proportional to the difference of the gravitational potential difference $U(x_1) - U(x_0)$. This equality of clock rates has been tested for various combinations of

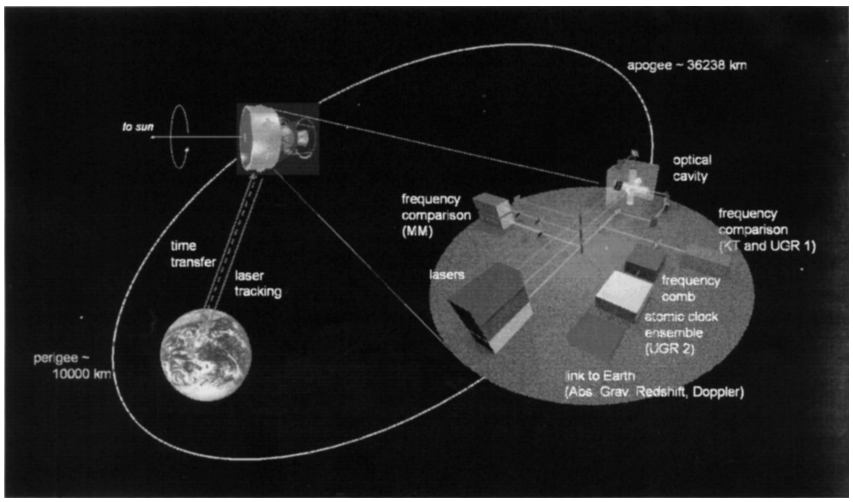

Figure 5. The mission scenario (apogee and perigee heights measured from Earth's surface).

clocks: for Cesium atomic fountain clock vs. H–maser with $2.1 \cdot 10^{-5}$ accuracy, for superconducting microwave resonator clocks vs. a H–maser clock (hf transition) with $1.7 \cdot 10^{-2}$ accuracy [5], and for an optical resonator vs. an electronic transition of the I_2 molecule with $2 \cdot 10^{-2}$ accuracy [55].

The OPTIS mission also aims at a test of the universality of this gravitational redshift, that is the equality of α_{clock} for different clocks, $|\alpha_{\text{clock2}} - \alpha_{\text{clock1}}|$. Due to the various clocks onboard of the OPTIS satellite also various combinations can be tested. Again, the high elliptic orbit, the mission time as well as the number of clocks will lead to an improvement of previous results by up to three orders.

4.2.3. Testing Metric Theories of Gravity

Tests of this kind are best described within the PPN-formalism [24, 56] which is a formalism to investigate the equations which determine the space–time metric $g_{\mu\nu}$ ($\mu, \nu = 0, \ldots, 3$) from the matter content in the universe. The method is first to identify the various matter and energy sources (both have to be treated on equal footing due to SR) and second to relate these various sources in a combinatorial way to the 10 independent metric coefficients. Each of these combinations is connected with a certain coefficient. A specific set of these coefficients singles out Einstein's field equations.

In local Lorentz invariant theories the PPN expansion of the different components of the metric tensor are given in terms of an isolated slowly rotating mass

$$g_{00} = -1 + 2\frac{U}{c^2} - 2\beta\frac{U^2}{c^4} \tag{41}$$

$$g_i := g_{0i} = 4\mu\frac{(\boldsymbol{J} \times \boldsymbol{r})_i}{c^3 r^3} \tag{42}$$

$$g_{ij} = (1 + 2\gamma)\frac{U}{c^2} \tag{43}$$

where $U(\boldsymbol{x}) = G \int \frac{\rho(\boldsymbol{x}')}{|\boldsymbol{x}-\boldsymbol{x}'|} d^3x'$ is the Newtonian potential and $\boldsymbol{J}$ the Earth's angular momentum. β describes the nonlinearity of GR, γ the strength of curvature. The parameter μ in (42) has been introduced to test gravitomagnetic effects [57], however in the 10–parameters PPN formalism μ is just a function of the PPN parameters γ and α_1. For Einstein's GR the parameters take the values $\beta = \gamma = \mu = 1$. Recently, in certain string theory induced dilaton models, a deviation of β and γ from their GR values in the range $|\beta - 1| \sim 5 \cdot 10^{-8}$ and $|\gamma - 1| \sim 4 \cdot 10^{-5}$ have been predicted [58].

The metric (41–43) is now used to describe various effects on test bodies: the gravitational redshift, the motion of point–like bodies and thus the Einstein pericentre shift or the Lense–Thirring effect, for example. These effects depend on

the PPN parameters and thus may be used so single out Einstein's GR from all other possibilities. By specifying the Newtonian potential, we also treat modifications of the gravitational field in the form of a Yukawa potential.

4.2.4. The Lense-Thirring Effect

Effects due to the rotation of a gravitating body, or gravitomagnetic effects, are absent in Newtonian gravity but occur in GR. Therefore these effects are particularly important for testing GR. There are two main gravitomagnetic effects: the precession of the orbit of a satellite, also called Lense-Thirring effect [59], and the dragging of inertial frames, also called the Schiff effect [60]. While the first effect is a global effect acting on the orbital plane of a satellite orbiting the rotating Earth, the second effect acts locally on gyroscopes. In metric theories of gravity, both effects are due to the same gravitomagnetic field whose source is the proper angular momentum $\boldsymbol{J}$ of the central mass which acts as source of the gravitational field. In its local version, the effect on the orientations of the spins $\boldsymbol{S}$ of four freely orbiting superconducting gyroscopes is $\dot{\boldsymbol{S}} = \boldsymbol{\Omega} \times \boldsymbol{S}$ with $\boldsymbol{\Omega} = -\frac{1}{2}\nabla \times \boldsymbol{g}$ and should be tested, among other things, by the GP–B mission [61], whose launch is scheduled for 2004, at a claimed accuracy level of the order of 1% or better. In the global version the whole orbit of the satellite, which is described by the equation of motion $\ddot{\boldsymbol{x}} = \nabla U - 2\dot{\boldsymbol{x}} \times \Omega$, can be thought of as a giant gyroscope whose node Ω and perigee ω undergo the Lense–Thirring secular precessions[11]

$$\dot{\Omega}_{\mathrm{LT}} = \frac{2GJ}{c^2 a^3 (1-e^2)^{\frac{3}{2}}}, \tag{44}$$

$$\dot{\omega}_{\mathrm{LT}} = -\frac{6GJ\cos I}{c^2 a^3 (1-e^2)^{\frac{3}{2}}}, \tag{45}$$

where I is the inclination of the orbital plane to the Earth's equator. Since 1996 this kind of measurement of the gravitomagnetic effect has been carried through by analysing the laser–ranging data of the geodetic satellites LAGEOS and LAGEOS II (see [8, 62] for the latest reports). The claimed accuracy is of the order of 20%–30%. There is a proposed LAGEOS III–LARES project whose originally proposed observable is able to measure the Lense-Thirring effect with about 1% accuracy [63, 64]. OPTIS is projected to be able to reach an accuracy of about 0.1%.

Indeed, the present status of our knowledge of the Newtonian part of the terrestrial gravitational field would allow to use a suitable combination of the nodes

[11] In the original paper by Lense and Thirring the longitude of the pericentre $\varpi = \Omega + \omega$ is used instead of ω.

of the existing LAGEOS and LAGEOS II and of OPTIS, in the LARES orbital configuration, as observable [9]. According to the recently released GGM01C Earth gravity model, based also on the first data from GRACE, the systematic relative error due to the unmodelled even zonal harmonics of geopotential would amount to 6×10^{-5}. Note that, since the gravitoelectric force (and the Yukawa-like force as well) does not induce any secular effect on the node, the proposed combination would be able to single out just the Earth gravitomagnetic field. Then, the so obtained results for the Lense–Thirring effect could be used for subsequent tests of post-Newtonian gravity.

4.2.5. The Gravitoelectric Einstein Pericentre Shift

Another interesting effect which could be measured in the gravitational field of Earth with a rather eccentric satellite orbit is the well known post–Newtonian gravitoelectric Einstein advance of the perigee of the orbit of a test body [57, 65]. Within the PPN weak field approximation this effect is

$$\dot{\omega}_{\mathrm{GE}} = \frac{2 + 2\gamma - \beta}{3} \frac{3nGM}{c^2 a(1 - e^2)} . \tag{46}$$

The quantity $n = \sqrt{\frac{GM}{a^3}}$ is the Keplerian mean motion. In [15] it is reported that the obtainable accuracy with a suitable combination of the nodes of LAGEOS and LAGEOS II and the perigee of LAGEOS II is of the order of 10^{-3}. In [16] the possibility of using the perigee of LAGEOS II only is examined; the obtainable accuracy is 2% over an observational period of 7 years. OPTIS will also be sensitive to this effect with one order of magnitude improved accuracy.

Note that such test should be performed after that the Lense-Thirring effect, which affects also the perigee, has independently been measured with the previously mentioned three-nodes combination; the data should be re-analyzed including the gravitomagnetic force at the level of accuracy released by the previous test in the force models of the equations of motion in the orbital processor softwares. Note also that it is not possible to disentangle the post-Newtonian gravitoelectric and Yukawa-like effects with only the OPTIS drag-free perigee[12] at our disposal. So, in the equations of motion of the orbital processors also the Yukawa-like acceleration would be included at the present-day level of accuracy obtained in the other past and independent tests. The so obtained measurement of

[12] The perigee of the Earth artificial satellites is very sensitive to a whole set of tiny but insidious non-gravitational perturbations. E.g., according to [12], it would be their action on the perigee of LAGEOS II that would make not entirely reliable the performed LAGEOS-LAGEOS II Lense-Thirring test. So, a possible solution like using the perigees of, say, LAGEOS II and OPTIS in order to constrain the gravitoelectric and the Yukawa effects independently of each other might be judged rather unreliable.

the gravitoelectric advance would be affected also by the systematic error due to the present-day level of accuracy in the knowledge of the Yukawa-like force [11].

4.2.6. Test of the Newtonian $1/r$-Potential

The satellite's motion is also sensitive to hypothetical deviations from the standard very weak field Newtonian $1/r$–potential, e.g. in the hypothesis of a Yukawa–like fifth force $U = \frac{GM}{r}\left(1 + \alpha e^{-\frac{r}{\lambda}}\right)$ where α is the strength and λ the range of the Yukawa part of the gravitational potential. The non-Newtonian part would induce a secular trend on the perigee of a near-Earth satellite given by [15, 63]

$$\dot{\omega}_{\text{Yukawa}} = \alpha \frac{n}{(1-e^2)^{\frac{3}{2}}}. \tag{47}$$

The strength α vanishes in Newtonian gravity. In [15] it has been shown that the systematic error in the measurement of α by means of a suitable combination of the nodes of LAGEOS and LAGEOS II and of the perigee of LAGEOS II would be of the order of 10^{-11} over 5 years. However, the impact of the non-gravitational perturbations of thermal origin [66] has not been included in that analysis. In [16] the possibility of using the perigee of LAGEOS II only is examined; the obtainable accuracy is $\sim 4 \times 10^{-10}$ over an observational period of 6–7 years. Note that this test should be conducted by considering the gravitomagnetic and gravitoelectric effects as fixed; the accuracy in their knowledge contributes to constraining the possible Yukawa signature.

5. SCIENCE REQUIREMENTS

5.1. Summary of Requirements

In order to meet the planned accuracy of tests and measurements, the scientific payload, the tracking and ranging systems as well as the drag-free Attitude and Orbit Control System (AOCS) have to fulfill the following requirements:

Residual accelerations: Accelerations will distort the resonator and thus lead to unwanted signals. In order to keep the accuracy stated in the science goals, residual, unmodellizable accelerations must be below 3×10^{-10} m/s^2. This can be achieved with drag–free techniques already available.

Residual rotations: Unknown rotations also will distort the resonator and, thus, have to be constrained to within $4 \cdot 10^{-4}$ Hz.

Temperature stability: Changes in the temperature of the optical resonator will lead to reduced accuracy. Suppression of these fluctuations to the aimed

accuracy requires a temperature stabilization at a level of about 10^{-5} μK. This is the most challenging technical task of this mission.

Laser lock stability: Drifts of the laser-to-cavity lock and mechanical misalignments of the laser beam into the resonator must be reduced to appropriate levels.

Tracking accuracy: Today, Earth bound satellites can be laser–tracked with an accuracy of a few cm. This is sufficient for the science goals given above. Current development in laser tracking may lead to an accuracy of a few mm in the near future. This would lead to further improvements of the tests 7, 8, and 9. Improvements in laser tracking accuracy are independent of the OPTIS mission and can be applied even during the operation of the mission.

5.2. Study of Systematic Errors

From the relation $\nu = \frac{n}{2L}c$ it is clear that any uncontrolled change in the length L of the cavity leads to an unwanted systematic effect. These effects may depend on the averaging time τ. Therefore, the sensitivity is given by (white noise is assumed for all time-dependent quantities)

$$\frac{(\Delta_{\max} c)(\tau)}{c} = \frac{1}{\sqrt{N}} \sqrt{2\left(\frac{\sigma_{\text{lock}}(\tau)}{\nu}\right)^2 + \left(\frac{\sigma^L_{\text{temp}}(\tau)}{L}\right)^2 + \left(\frac{\sigma^L_{\text{accel}}(\tau)}{L}\right)^2} \tag{48}$$

where N is the number of runs and $\sigma(\tau)$ denote the Allan–variance [67] of the various quantities. In particular, $\sigma_{\text{lock}}(\tau)$ is the Allan–variance of the lock of a laser to its respective cavity, $\sigma^L_{\text{temp}}(\tau)$ is the Allan–variance of the length of a single cavity, or, in the case of the test of the isotropy of the velocity of light, of the difference of the lengths of the two resonators affected by temperature variations, and $\sigma^L_{\text{temp}}(\tau)$ the corresponding quantity for residual accelerations. In this discussion we neglect possible creep of the resonators. The relevant averaging time depends on the type of experiment: for the isotropy test, the time scale is given by the spin period of the satellite, which we take to be between 100 and 1000 s. For the constancy of the speed of light test, the orbit period provides the time scale $\tau = 7$ h. The Allan–variance of the reference clock has to be added to (48) in this case.

Due to the science goals, the individual contributions to the total errors have to be smaller than 10^{-18} on the timescale of the corresponding test. We require

Isotropy of speed of light: $\frac{1}{\sqrt{N}}\frac{\sigma_{\text{lock}}}{\nu} \le 10^{-18}$, $\frac{1}{\sqrt{N}}\frac{\sigma^{\Delta L}_{\text{temp}}}{L} \le 10^{-18}$, and $\frac{1}{\sqrt{N}}\sigma^{\Delta L}_{\text{accel}} L \le 10^{-18}$ in the range $\tau = 100, \ldots 1000$ sec.

Constancy of speed of light: $\frac{1}{\sqrt{N}}\frac{\sigma_{\text{lock}}}{\nu} \le 10^{-15}$, $\frac{1}{\sqrt{N}}\frac{\sigma^L_{\text{temp}}}{L} \le 10^{-15}$, $\frac{1}{\sqrt{N}}\frac{\sigma^L_{\text{accel}}}{L} \le 10^{-15}$, and $\sigma^{\text{clock}}/\nu_{\text{clock}} \le 10^{-15}$ in the range $\tau = 7$ h.

UGR with atomic clocks: $\sigma^{\text{clock}}/\nu_{\text{clock}} \leq 1 \cdot 10^{-16}$.
UGR with atomic clocks and resonator: $\sigma^{\text{clock}}/\nu_{\text{clock}} \leq 10^{-16}$.

5.3. Thermal Stability

A high thermal stability of the resonator is mandatory for the success of this mission. Temperature variations lead to variations of the length of the resonator and, thus, to systematic errors. We now analyze how constant the temperature has to be in order to reach the science goal. Taking a particular temperature T_0 as reference, then the length of a body changes with the temperature according to

$$L(T) = L(T_0)(1 + \beta(T_0)(T - T_0) + \beta_2(T_0)(T - T_0)^2 + \ldots). \tag{49}$$

The β's are the thermal expansion coefficients of first and second order. Accordingly, the materials should have very small thermal expansion coefficients at room temperature (for budgetary reasons we want to avoid cryogenic techniques as used, e.g., for GP-B and planned for STEP). Suitable materials for that purpose are ULE glass or silicon. ULE has $\beta \simeq 10^{-9}$ K^{-1} and Silicon $\beta = 4 \cdot 10^{-6}$ K^{-1} at room temperature. Moreover, Silicon has a vanishing first order expansion coefficient at $T_0 \approx 140$ K: $\beta^{(\text{Si})}(140\text{ K}) = 0$ and $\beta_2^{(\text{Si})}(140\text{ K}) = 2 \cdot 10^{-9}$ K^{-2}. Consequently, the science goals require that the overall temperature stability for ULE at $T = 273$ K must reach $\Delta T \leq 10^{-9}$ K. For Silicon at $T_0 = 140$ K we only need $\Delta T \leq 10^{-7}$ K assuming an offset of 10 mK from the zero–crossing temperature. The actual temperature instability may be larger by $\sqrt{N}$, as long as the temperature fluctuations are are not correlated to the orbital or rotational frequency of the satellite. For the isotropy experiment with one turn in about 1000 s and an one–year operation time, $\sqrt{N} \sim 170$ so that the actual temperature requirements are relaxed by more than two orders, $\sigma^L_{\text{temp}}(1000\text{ s}) \leq 0.2\ \mu$K for ULE and $\sigma^L_{\text{temp}}(1000\text{ s}) \leq 20\ \mu$K for Si at 140 K. For the constancy of the speed of light and UGR tests for one–year operation, $\sqrt{N} \sim 25$, so that the requirements are relaxed by more than one order, that is, $\sigma^T(7\text{ h}) \leq 0.02\ \mu$K for ULE and $\sigma^T(7\text{ h}) \leq 2\ \mu$K for Si at 140 K.

5.4. Stability of Laser Lock

The stability requirements of the laser lock can be met by appropriate technology, as described below in the technology sections.

5.5. Residual Acceleration and Rotation, Gravity Gradient

Here we have to determine the influence of accelerations and rotations on the shape of the resonator. At first we mention that there is always some residual

(unknown) acceleration and rotation which, however, can be minimized by an appropriate drag-free control scheme to a very low level. Second, accelerations and rotations are always induced by the gravity gradient which is present everywhere on an extended body. These effects can be calculated. The extension of the body leads to an extra force and torque resulting in a non-geodesic motion of the center-of-mass coordinate and a rotation of the body which both lead to a distortion of the body according to its elastic properties. Furthermore, the gravity gradient also will distort the body. Though all effects in general depend on each other (an elastic deformation of the body leads to other extra forces) we can treat them separately because each of these effects is very small. As a result, we show that the optimum design for the resonators consists of a cubic or spherical shape. In this case all accelerations and torques resulting from a gravity gradient vanish to high order.

In the following the center of mass of the resonator is assumed to be the drag-free point of the satellite. This can be achieved if the satellite is equipped with two accelerometers whose acceleration is actively controlled to zero.

The results of the two following subsections partly depend on each other. In the first part we show that a cubic or spherical symmetry is preferred for a good realization of a force- and torque-free motion, in the second part we calculate the maximum residual acceleration and rotation for such a body. Also the influence of the gravity gradient on the shape of the body is calculated.

5.5.1. Extended Body: Gravity Gradient Induced Acceleration and Rotation

Acceleration. In a Newtonian framework (there is no need for a relativistic treatment of this problem) the gravitational force acting on an extended solid body with mass–density $\rho(\boldsymbol{x})$ in a general inhomogeneous gravitational field with potential $U(\boldsymbol{x})$ is

$$\boldsymbol{F} = \int \rho(\boldsymbol{x}) \boldsymbol{\nabla} U(\boldsymbol{x}) d^3x \,. \tag{50}$$

The center-of-mass coordinate $\boldsymbol{x}_{\mathrm{com}}$ defined by $m\boldsymbol{x}_{\mathrm{com}} = \int \rho(\boldsymbol{x}) \boldsymbol{x} d^3x$, satisfies the equation of motion

$$m\ddot{\boldsymbol{x}}_{\mathrm{com}} = m\boldsymbol{\nabla} U(\boldsymbol{x}_{\mathrm{com}}) + \frac{1}{2}\boldsymbol{\nabla}\left(\theta^{ij}\partial_i\partial_j U(\boldsymbol{x}_{\mathrm{com}})\right) + \ldots \,, \tag{51}$$

where $m = \int \rho(\boldsymbol{x}) d^3x$ is the total mass and where $\boldsymbol{\nabla}$ acts on the center–of–mass coordinate only. Here the quantity θ^{ij} is the tensor of inertia

$$\theta^{ij} := \int \rho(\boldsymbol{x})\left(\boldsymbol{x}_{\mathrm{rel}}^2 \delta^{ij} - x_{\mathrm{rel}}^i x_{\mathrm{rel}}^j\right) d^3x_{\mathrm{rel}} \tag{52}$$

with the relative coordinate $\boldsymbol{x}_{\mathrm{rel}} = \boldsymbol{x} - \boldsymbol{x}_{\mathrm{com}}$. The dots in Eq. (51) indicate further terms of order $m\boldsymbol{\nabla}(x_{\mathrm{rel}}^n \partial^n U(\boldsymbol{x}_{\mathrm{com}}))$, $n \geq 3$. In the case of a spherically symmetric

gravitational field generated by a mass M these terms are of order $m\frac{GM}{x_{\rm com}^2}(\frac{x_{\rm rel}}{x_{\rm com}})^n$. In orbit, $GM/x_{\rm com}^2 \sim 10\ {\rm m/s^2}$ and $x_{\rm rel}/x_{\rm com} \sim 10^{-8}$ for a rigid body of 10 cm extension. Consequently, the second therm of Eq. (51) is $\sim 10^{-16}$ smaller than the first term and the next term is even 24 orders smaller. For a body of 1 kg mass, the second term amounts to an acceleration of $\sim 10^{-15}\ {\rm m/s^2}$.

Eq. (51) shows that an inhomogeneous gravitational field leads to a non-geodesic motion of the center-of-mass coordinate. The extra force is given by the second and further terms. Due to the drag–free motion of the satellite which is provided by highly sensitive accelerometers and highly accurate microthrusters, the first term in (51) vanishes to high accuracy in the drag free point, while the second gives rise to a force on the experimental payload which in turn may lead to a distortion of e.g. the resonator. This has either to be taken into account in the data analysis or has to be minimized by an appropriate design of the resonator.

Rotation. An inhomogeneous gravitational field not only gives an extra force but also a torque acting on the rigid body. This torque with respect to the center-of-mass position is given by

$$\boldsymbol{T}(\boldsymbol{x}_{\rm com}) = \int \rho(\boldsymbol{x})\boldsymbol{x}_{\rm rel} \times \boldsymbol{\nabla} U(\boldsymbol{x}) d^3x \tag{53}$$

and leads to

$$T^i(\boldsymbol{x}_{\rm com}) = \epsilon^{ijk}\partial_k \left(\theta^{jl}\frac{\partial U(\boldsymbol{x}_{\rm com})}{\partial x^l}\right) + \dots . \tag{54}$$

This term is of the order $m\frac{GM}{x_{\rm com}^2}x_{\rm rel}\frac{x_{\rm rel}}{x_{\rm com}}$; for the same specifications as above this is $\sim 10^{-8}\ {\rm kg\,m^2/s^2}$. The next term, indicated by the dots in Eq. (54), is smaller by a factor 10^{-8} and can be safely neglected. The torque induces an angular acceleration $\dot{\omega} \sim \nabla^2 U(\boldsymbol{x}_{\rm com})$ which is of the order $10^{-6}\ {\rm s^{-2}}$. Since the orientation of the satellite is such that its spinning axis is always directed towards the Sun, a counter–torque will be acted upon the rigid body. This leads to a position dependent acceleration of the order $a_{\rm torque} \sim x_{\rm rel}\dot{\omega}$ which for our specifications is about $10^{-7}\ {\rm m/s^2}$. The next terms are smaller by eight orders of magnitude.

To be more accurate, the angular acceleration $\dot{\omega}$ can best be determined in the local coordinate system in which the tensor of inertia is diagonal, $\theta^{ij} \stackrel{*}{=} {\rm diag}(\theta^1, \theta^2, \theta^3)$. In terms of the components ω_i of the angular velocity in these coordinates, we can express the torque as

$$T^i \stackrel{*}{=} \theta_i\dot{\omega}_i + \sum_l \sum_j \epsilon_{ijl}\theta_l\omega_l\omega_j . \tag{55}$$

If we insert the torque derived above, we get the equation of motion

$$\theta_i \dot{\omega}_i + \sum_{l,j} \epsilon_{ijl} \theta_l \omega_l \omega_j \stackrel{*}{=} \sum_{j,k} \epsilon^{ijk} \theta_j \partial_k \partial_j U(\boldsymbol{x}_{\rm com}) \,. \tag{56}$$

In the same coordinate system Eq.(51) reduces to

$$m \ddot{\boldsymbol{x}}_{\rm com} \stackrel{*}{=} m \nabla U(\boldsymbol{x}_{\rm com}) + \frac{1}{6} \nabla \left(\sum_k \theta_k \partial_k^2 U(\boldsymbol{x}_{\rm com}) \right) . \tag{57}$$

From the last two equations it can bee seen, that in the case of a rigid body whose diagonal elements in all three directions are the same, $\theta^1 = \theta^2 = \theta^3$, the first non-trivial terms due to the extendedness of the body vanish

$$m \ddot{\boldsymbol{x}}_{\rm com} \stackrel{*}{=} m \nabla U(\boldsymbol{x}_{\rm com}) + \mathcal{O}((x_{\rm rel}/x_{\rm com})^3) \tag{58}$$

$$T^i \stackrel{*}{=} 0 + \mathcal{O}((x_{\rm rel}/x_{\rm com})^2) \,. \tag{59}$$

Thus, this analysis shows that a mass distribution of the cavity structure should be of cubic or of spherical symmetry[13].

5.5.2. Elastic Body: Distortions due to Accelerations, Rotations and Gravity Gradient

Definitions. Elastic distortions of a body are appropriately described by the connection of the stress tensor of the body with the distortion tensor

$$T^{ij} = C^{ijkl} S_{kl} \,, \tag{60}$$

where C^{ijkl} are the elasticity coefficients of the body under consideration, see e.g. [68]. This equation is valid in a non-rotating frame attached to the body. The tensor C^{ijkl} is symmetric in the first and second pair of indices and under the exchange of the first and second index pairs and, thus, in general possesses 21 independent coefficients[14]. The distortion or strain tensor is defined by

$$S_{kl} = \frac{1}{2} \left(\partial_l \xi_k + \partial_k \xi_l \right) \,, \tag{61}$$

[13] If the monolithic resonator slightly deviates from a cubical form with one side L_z being slightly different from the other two sides $L_x = L_y$, then the additional force is $\frac{m}{12}(L_x^2/x_{\rm com}^2)\frac{GM}{r_{\rm com}^2}(L_z^2 - L_x^2)/L_x^2$. This term is smaller than the leading term by a factor $\frac{1}{12}(L_x^2/x_{\rm com}^2)(L_z^2 - L_x^2)/L_x^2 \sim 10^{-16}(L_z^2 - L_x^2)/L_x^2$. This poses no problem for fulfilling the requirement $|a| \leq 3 \cdot 10^{-11} g$ (see below). Furthermore, due to the torque a nonsymmetrical body experiences an additional angular acceleration $\dot{\omega} \sim \frac{\Delta\theta}{\theta} \partial^2 U$. Since the resulting acceleration $a_{\rm torque} \sim x_{\rm rel} \dot{\omega}$ should be smaller than $3 \cdot 10^{-10}$ m/s^2, the differences in the diagonal parts of the inertial tensor should be restricted by $|\Delta\theta/\theta| = |(L_z^2 - L_x^2)/L_x^2| \leq 10^{-2}$, that is, $|(L_z - L_x)/L_x| \leq 5 \cdot 10^{-3}$. This is easily achieved.

[14] The contact to conventional notation is made by replacing the index pairs according to $xx \leftrightarrow 1$, $yy \leftrightarrow 2$, $zz \leftrightarrow 3$, $xy \leftrightarrow 4$, $xz \leftrightarrow 5$, $yz \leftrightarrow 6$. Then $C^{yzxx} = C_{31}$, for example.

where the elongations $\xi^i = x^i(t) - x^i(0)$, that is, the difference of the position $x^i(t)$ of the small mass elements of the body at time t with respect to its initial position $x^i(0)$. Eq. (60) is a generalization of Hooke's law. The equation of motion of the small mass elements of the body is given by the divergence of the total stress tensor

$$\rho\ddot{\xi}^i = \partial_j \overset{\text{tot}}{T}{}^{ij}\,, \tag{62}$$

where the total stress tensor consists of the elastic part, the friction and external forces

$$\overset{\text{tot}}{T}{}^{ij} = T^{ij} + \overset{\text{fric}}{T}{}^{ij} + \overset{\text{force}}{T}{}^{ij}. \tag{63}$$

For vanishing friction and with a gravitational force which is the gradient of the Newtonian potential and an external force density k_i which may represent residual accelerations, the equation of motion reads

$$\rho\ddot{\xi}^i = \partial_j T^{ij} - \rho\partial_i U + k_i\,. \tag{64}$$

Using the expression for the distortion tensor we get

$$\rho\ddot{\xi}^i = C^{i(jl)k}\partial_j\partial_l\xi_k - \rho\partial_i U + k_i\,. \tag{65}$$

In the case that the body is—due to some forces—at rest in the observer frame, or in situations with adiabatic changes in time, this equation reduces to

$$0 = C^{i(jl)k}\partial_j\partial_l\xi_k + \rho\partial_i U + k_i\,. \tag{66}$$

We use this equation and

$$\begin{aligned} U_{\text{com}}(\delta\boldsymbol{r}) &= U(\boldsymbol{x}) - U(\boldsymbol{x}_{\text{com}}) \\ &= \frac{GM}{r_{\text{com}}^3}\delta x_{\text{rel}}^2(\sin^2\theta - 2\cos^2\theta) \\ &= \frac{GM}{r_{\text{com}}^3}(x^2 + y^2 - 2z^2) \end{aligned} \tag{67}$$

where θ is the angle between $\boldsymbol{r}_{\text{com}}$ and $\boldsymbol{x}_{\text{rel}}$, in order to calculate first the stress tensor influenced by the external force and by the gravity gradient and then, from (61), the distortions ξ^i. Fig. 6 (left) gives a visualization of the potential and the corresponding force field.

Isotropic and Homogenous Materials. For simplicity, we assume the body to be made of homogeneous and isotropic materials. In this case the relation between the distortion tensor and the stress tensor simplifies to

$$T^{ij} = \lambda\delta^{ij}S + 2\mu S_{ij} \tag{68}$$

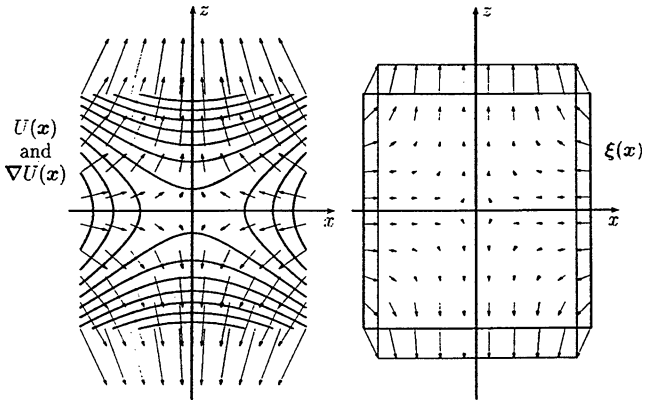

Figure 6. Distortion of the cavity in a gravity gradient field of Eq. (67). Left: Equipotential surfaces and the corresponding force field in the center-of-mass system. Right: the displacement field of an elastic homogeneous and isotropic cube (black: original form, red: distorted form).

where S is the trace of S_{ij}. Also

$$S_{ij} = \frac{1+\nu}{E} T^{ij} - \frac{\nu}{E} \delta_{ij} T \tag{69}$$

where T is the trace of T^{ij}. λ and μ are Lamé's constants (μ is also called the shear modulus), E is Young's modulus, and ν the Poisson number (not to be confused with the frequency).

Now we treat each problem separately: (i) the distortion induced by the external force, and (ii) the distortion induced by the gravity gradient. What follows is, of course, only a rough estimate; for a more refined consideration one has to take into account the possibly non–isotropic structure of the cavity material (in the case of Silicon, for example), and the presence of cylindrical holes in the cube. This certainly cannot be done analytically so that numerical finite element methods have to be employed.

Residual External Force. This is a standard problem and can be solved easily. If the normals of the faces of a cube with length L are in direction of the coordinate axes, then a force F acting along the axes, we then have to consider the length deformation in z-direction (strain), $\Delta L_z/L = S_{zz}$, and the transverse contraction $\Delta L_x/L = S_{xx} = S_{yy} = \Delta L_y/L$. Since in this case $T^{xx} = T^{yy} = 0$, we get from (69)

$$\frac{\Delta L_z}{L} = \frac{1}{E} T^{zz} = \frac{1}{E} \frac{F}{L^2}, \tag{70}$$

$$\frac{\Delta L_x}{L} = -\frac{\nu}{E} T^{zz} = -\frac{\nu}{E}\frac{F}{L^2}. \tag{71}$$

Since the Poisson number always is between 0 and 0.5, $\Delta L_x/L$ is always smaller than $\Delta L/L$ so that any requirement for $\Delta L/L$ also fulfills all requirements for $\Delta L_x/L$. In the OPTIS set-up a cubical geometry for the resonator is used, so that we can replace $F = ma$ with $m = \rho L^3$ and where a is a residual acceleration

$$\frac{\Delta L_z}{L} = \frac{1}{E}\frac{\rho L^3 a}{L^2} = \frac{\rho L a}{E}\,. \tag{72}$$

Any force, either in direction of the cavity axis or orthogonal to it, should lead to a variation of the length $\Delta L_z/L$ smaller than 10^{-18}.

We discuss this for Silicon and ULE. Since Silicon has cubic crystalline symmetry, it possesses three elastic constants C_{11}, C_{12}, and C_{44}. In order to be on the safe side, for the first rough estimate we take the smallest one, namely $C_{12} =$ 65 Gpa. All other characteristic numbers for Silicon, the other elastic constants as well as Young's, bulk and shear modulus are larger by up to a factor of two. For ULE only Young's modulus is known, with a value between 67 and 90 GPa. Therefore, an $E = 60$ GPa is a safe lower limit to the elastic constants for both materials and, at least as the influence of residual accelerations and rotations and the gravity gradient is concerned, there is no preference for one of these materials. Furthermore, the densities of Silicon as well as for ULE are approximately the same: $\rho \approx 2.3$ g/cm^3. Then, from $\Delta L/L \leq 10^{-18}$ and a length L of the order 5 cm we get the requirement $|a| \leq 1.5 \cdot 10^{-10}$ m/s^2 on the residual acceleration on a time scale of about 1 year.

This result can be used to estimate the maximum allowable difference between the drag–free point and the center-of-mass of the resonator. Denoting this difference by $\delta\boldsymbol{r}$, then the resulting acceleration $a^i = \delta r^j \partial_i \partial_j U$ acting on the resonator turns out to be $\boldsymbol{a} = 2\frac{GM}{r_{\rm com}^3}\delta r(\sin\vartheta\,\boldsymbol{e}_x - 2\sin\vartheta\,\boldsymbol{e}_z)$ where ϑ is the angle between $\delta\boldsymbol{r}$ and the z-axis. From this it follows that the displacement δr must be smaller than 0.1 mm. The drag–free point must coincide with the center-of-mass of the monolithic resonator to within 0.1 mm. This is technically feasible.

Gravity Gradient. For a homogeneous and isotropic body in a static situation in a gravitational field, the displacement vector obeys the equation

$$\Delta\boldsymbol{\xi} + \frac{1}{1-2\nu}\boldsymbol{\nabla}(\boldsymbol{\nabla}\cdot\boldsymbol{\xi}) + \frac{\rho}{\mu}\boldsymbol{\nabla}U = 0\,. \tag{73}$$

For the solution we make the ansatz [69] $\boldsymbol{\xi} = \boldsymbol{\nabla}\psi$ and get

$$\boldsymbol{\nabla}\left(\frac{2(1-\nu)}{1-2\nu}\Delta\psi + \frac{\rho}{\mu}U\right) = 0\,, \tag{74}$$

which leads to

$$\Delta\psi = -\frac{1-2\nu}{2(1-\nu)\mu}\rho U\,. \tag{75}$$

With the potential (67) we immediately get the solution

$$\psi = \frac{1-2\nu}{24(1-\nu)\mu}\rho\frac{GM}{r_{\text{com}}^3}\left(-x^4-y^4+2z^4\right)\,, \tag{76}$$

so that the displacement vector reads

$$\boldsymbol{\xi} = \frac{1-2\nu}{6(1-\nu)\mu}\rho\frac{GM}{r_{\text{com}}^3}\left(-x^3\boldsymbol{e}_x - y^3\boldsymbol{e}_y + 2z^3\boldsymbol{e}_z\right)\,, \tag{77}$$

see Fig. 6 (right) for a visualization of the deformation of a cube. This result does not depend on the orientation of the body.

This result gives the maximum strain of the resonator in z–direction by computing the z-component of $\boldsymbol{\xi}$ for $(x, y, z) = (0, 0, \pm L/2)$

$$\frac{\Delta L}{L} = \frac{\xi_z(L/2)-\xi_z(-L/2)}{L} = \frac{1-2\nu}{12(1-\nu)\mu}\rho\frac{GM}{r_{\text{com}}^3}L^2\,, \tag{78}$$

which for a length of $L = 5$ cm gives $\Delta L/L \approx 0.8\cdot 10^{-18}$ at perigee. This satisfies the science requirement.

Residual Rotation. The same scheme can be used to calculate the distortion of bodies due to a constant rotation ω around its symmetry axis. In adapted cylindrical coordinates, the potential for the resulting radial force is $U = \frac{1}{2}\omega^2\tilde{\rho}^2$, where $\tilde{\rho}$ is the distance from the rotation axis. As above, we arrive for the function ψ at the equation

$$\Delta\psi = \frac{1-2\nu}{4(1-\nu)\mu}\rho\omega^2\tilde{\rho}^2. \tag{79}$$

The solution which is compatible with the condition $\psi \to 0$ for $\tilde{\rho} \to 0$ is given by $\psi(\tilde{\rho}) = \frac{1-2\nu}{64(1-\nu)\mu}\rho\omega^2\tilde{\rho}^4$. The resulting displacement vector is then given by

$$\boldsymbol{\xi} = \frac{1-2\nu}{16(1-\nu)\mu}\rho\omega^2\tilde{\rho}^3\boldsymbol{e}_\rho. \tag{80}$$

From this solution we can calculate the change in the diameter d of a cylinder

$$\frac{\Delta d}{d} = 2\frac{\xi_\rho(d/2)}{d} = \frac{1-2\nu}{64(1-\nu)\mu}\rho\omega^2 d^2. \tag{81}$$

With the requirement $\Delta d/d \le 10^{-18}$ and a diameter of 5 cm, the condition of a rotation–free point still allows a maximum residual rotation frequency of $\Delta\omega \le 10^{-4}$ Hz. In case of a given rotations, e.g. for test of the isotropy of c, the unknown residual rotation frequency can be relaxed.

The Rotation Point. For stabilization reasons and for the isotropy tests, the satellite is assumed to rotate at a rate of about 10^{-3} Hz. The condition $\Delta d/d \leq 10^{-18}$ allows an error δd in the location of the rotation point. For a given rotation rate, we get from $(\xi(d/2+\delta d)+\xi(d/2-\delta d))/d \leq 10^{-18}$

$$\delta d \leq \frac{10^{-9}}{\omega}\left(\frac{1-\nu}{1-2\nu}\frac{16\mu}{3\rho}\right)^{1/2}. \tag{82}$$

This is independent of the dimension of the resonator. For our specifications, we get $\delta d \leq 2\cdot 10^{-5}/\omega$[Hz] which can easily be achieved.

6. PAYLOAD AND MISSION RELEVANT TECHNOLOGIES

6.1. Optical Resonators

The resonators (cavities) are one of the essential parts of the experimental payload. Resonators are a realization of so-called light clocks. Locking of lasers to the resonators will give highly stabilized frequencies which carry, via $\nu = nc/(2L)$, where L is the length of the cavity, the information about the velocity of light c for propagation along the cavity axis. This information is used in order to make statements about the isotropy and the constancy of the speed of light. For this, the length of the cavity has to be very stable since otherwise this could mask the searched effect. For cryogenic resonators the stability is $\delta L/L \leq 7\cdot 10^{-16}$ [2].

There are many influences on the cavities: Temperature, temperature gradient, intertial forces like residual acceleration and centrifugal forces, gravitationally induced non–geodesic forces and torques, and the gravity gradient. In order to avoid accelerations induced by the gravity gradient on an extended body a cubic symmetry of the cavity is preferable, see Section 5.5.1. Therefore, we choose a design as shown in Fig. 7. The gravity gradient may also distort the cavity. Therefore a stiff material is preferred.

The high dimensional stability requires materials with small thermal expansion coefficients. For OPTIS the options are (i) ULE glass with thermal expansion coefficient of $\beta = 10^{-9}/\mathrm{K}$ at room temperature, or (ii) Silicon with a vanishing thermal expansion coefficient at 140 K and a second–order thermal expansion coefficient of $2\cdot 10^{-9}/\mathrm{K}^2$.

6.2. Lasers

The lasers should have a free running linewidth of no more than a few kHz, so they can probe the resonance of a cavity having a linewidth in the low kHz range. Requirements on the free running long term frequency stability are mild, but no shifts of the frequency should occur that are too large to be compensated for by the laser frequency lock system. Actuators for modulating and controlling

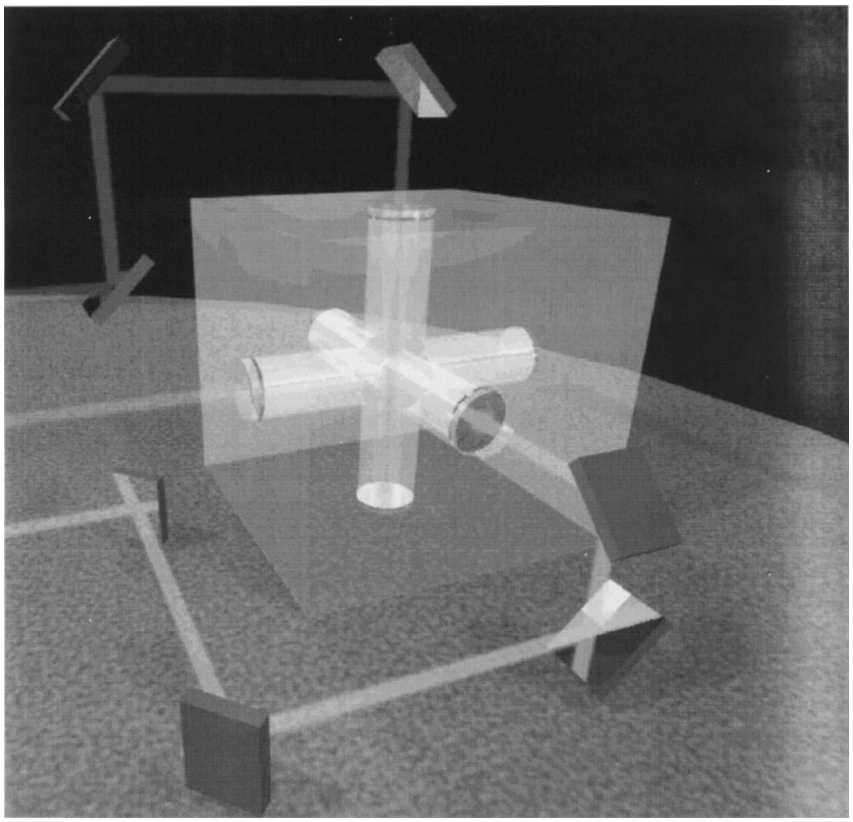

Figure 7. Design of cavities as a monolithic cubic block with the orthogonally oriented resonators.

the laser frequency are necessary. Beside that, they should meet the requirements for space operation.

All these requirements are met by monolithic, diode-pumped Nd:YAG lasers at a wavelength of $\lambda = 1064\,\text{nm}$, that are already available in space-qualified versions.

6.3. Laser Locking

The Allan variance of the error σ_{lock} of the laser frequency servo ("lock") electronics and optics scales with the linewidth B_{cav} of the cavity resonance, i.e. $\sigma_{\text{lock}} = \alpha_{\text{lock}} B_{\text{cav}}$, where α_{lock} is a dimensionless constant given by the properties of the setup. Thus, a low cavity linewidth $B_{\text{cav}} = c/(2L)/\mathcal{F}$ is highly desirable in

order to suppress the influence of lock errors. Here, L is the mirror spacing and $\mathcal{F}$ the cavity finesse. The influence of the gravity gradient increases for large L, so L is limited to about 5 cm. The finesse $\mathcal{F}$ is given by the quality of the dielectric mirrors; state-of-the-art mirrors on quartz substrates reach $\mathcal{F} \sim 10^6$. Thus, a linewidth of 1.5 kHz appears feasible. To have some margin, we assume $B_{\text{cav}} = 3\,\text{kHz}$ in the following. For a laser wavelength of 1 μm, i.e. a laser frequency $\nu \simeq 300\,\text{THz}$, the requirement of $\sigma_{\text{lock}}/\nu \sim 10^{-18}$ thus implies a requirement on $\alpha_{\text{lock}} \sim 10^{-7}$.

On the relevant timescales $\tau \gtrsim 100\,\text{s}$, the lock error is not due to any fundamental limitations such as quantum noise, but due to several causes of a rather mundane nature. Examples are residual amplitude modulation of the laser beams, parasitic reflections in the beam path between laser and resonator, temperature dependence of electronic circuits, laser power induced heating of the cavities, and technical noise of photodetectors. These influences must be tightly under control for achieving the required stability. The OCAMS technique [70] for detecting and compensating for various disturbances in frequency control systems will probably be useful.

Isotropy Experiments. Assuming, as above, a gain in sensitivity due to averaging by a factor of $\sqrt{N} \sim 170$ reduces the requirement *per measurement* to $\alpha_{\text{lock}} \sim 10^{-5}$. In the best present isotropy experiment, $\alpha_{\text{lock}} \sim 2 \cdot 10^{-6}$ has been achieved for $100\,\text{s} \lesssim \tau \lesssim 1000\,\text{s}$ [2, 71], although the setup was not even optimized for these time-scales. The requirement of the isotropy test can thus easily be fulfilled.

Other Experiments. The requirements on the lock system are stronger for the constancy of the speed of light and the UGR experiments: With a gain in sensitivity due to averaging by a factor of $\sqrt{N} \sim 25$, the requirement for the these test is $\alpha_{\text{lock}} \sim 3 \cdot 10^{-6}$ on a timescale of 7 h. For comparison, the corresponding figure in [45] was 10^{-4} at 6 h. However, this was mostly due to distortions of the setup (by several 100 μm) that changed the relative position of the lasers and the cavities.

Fiber coupling of the laser to the cavities can be used to minimize these influences, and it is probable that this will allow to meet the lock stability requirements. It is desirable to construct the laser–fiber as well as the cavity–fiber couplings as compact and rigid as possible. Mild requirements on temperature changes of the optical bench ($\lesssim 0.1^\circ$C) should be met to reduce thermal distortions.

6.4. Atomic Clocks

There are various atomic clocks available: H-maser, Rb- and Cs-clocks, and ion clocks based on Hg^+. Their precision in terms of the Allan deviation is shown

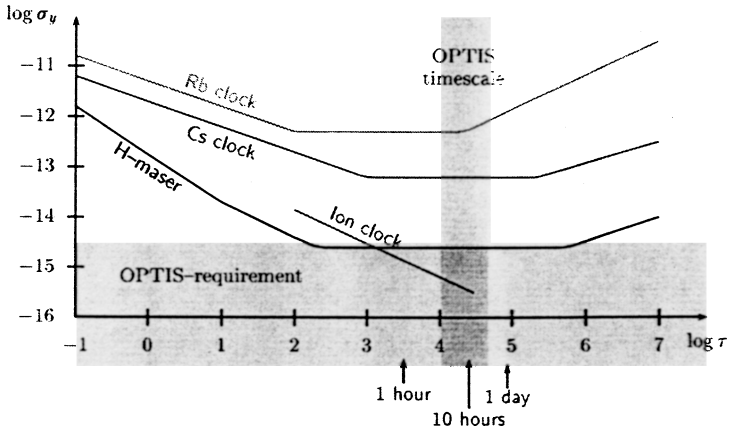

Figure 8. Typical Allan deviations σ_y/ν for Rb-, Cs-, Ion- and H-maser–clocks in comparison with the OPTIS requirements for the constancy of c test.

in Fig. 8. The type of clocks which meet the requirements of our mission are H–masers and ion–clocks.

H-Maser. H-masers are based on a hyperfine transition of the ground state of the hydrogen atom with a life time of about 1 s which is coupled to a resonator. The frequency is 1.420 405 751 Hz. A space-qualified active hydrogen maser has been developed for the ACES experiment on the ISS [54, 72]. Its instability is $2 \cdot 10^{-15}$ at 10000 s.

Ion Clocks. Ion clocks are based on hyperfine transitions of trapped ions (e.g. Hg^+, Cd^+, Yb^+). The Allan deviation can be as low as $7 \cdot 10^{-16}$ for an integration time of several hours [73]. The most promising candidate for an atomic clock for OPTIS appears at the present time to be an ionic clock.

6.5. Frequency Comb

The constancy of c and the UGR tests require a high-precision technique for comparing frequencies in the microwave and optical range, differing by some 5 orders of magnitude. The recently invented frequency comb is the appropriate technique, see [74] for an overview. This technique, which is simpler, cheaper, power-saving and more accurate than previous methods, could be used by OPTIS in space where the optical resonator–frequencies should be compared with the atomic microwave frequencies needed for the constancy of the speed of light test

and the test of UGR. OPTIS needs an accuracy of the frequency comparison of $3 \cdot 10^{-15}$. In the laboratory, an accuracy of 10^{-15} has already been achieved.

6.6. Thermal Isolation

The first step in the analysis of this problem and for providing the appropriate thermal stabilization is the analysis of the thermal conditions given by the orbit and the corresponding thermal properties inside the satellite in the case that we provide the satellite with superinsolation layers. The temperature outside the satellite during one orbit varies between –110 K and –50 K. In a first step the satellite is modelled as a cylindrical box. If we assume four superinsolation layers made of coated Capton film each being 20 mm thick leads to a temperature variation inside the satellite of around 20 mK. The thermal stability in the μK region as it follows from the science requirements has to be provided by an active shielding.

6.7. Gravity Reference Sensors

As the effects of SR and GR measured in the OPTIS experiments are very small, a highly disturbance–free environment is required for the success of the mission. In the last years so-called 'drag-free sensors' have been developed that offer the opportunity to cancel out, to a certain level of accuracy, all non-gravitational disturbance forces and torques (like air drag, solar pressure, magnetic field disturbances etc) on the orbiting satellite. Therefore drag-free sensors are used for very precise translational drag–free and attitude control. The control system implemented to achieve the disturbance–free environment is called Drag-Free and Attitude Control System (DFACS).

The original drag-free concept involves centering a free-floating test mass located inside a satellite. External forces and torques will move the satellite relative to the test mass. The change in the relative position is measured and then used to derive the appropriate control force which has to be applied by the DFACS in order to drive the test mass displacement to zero. Then the test mass is free of external disturbances and follows a purely gravitational orbit. Since the satellite is forced to follow the test mass, it too follows the same gravitational orbit.

There are several drag-free sensors available at the market today. One of their main features is the mode of operation. The two main operation modes could be called 'Accelerometer Mode' and 'Displacement Mode'.

The Displacement Mode concept uses a 'free-floating' test mass. The displacement of this test mass relative to the housing is measured by the sensor. This sensor signal is used to control the satellite to follow the test mass in order to drive the relative displacement to zero. In doing so the external disturbances on the test mass are minimised and the test mass—and thereby the satellite—will follow a

free-fall orbit. This mode provides a very high sensor accuracy. However, the acceleration is not directly accessible but has to be calculated from the displacement measurements.

In the Accelerometer Mode concept, the test mass is forced to follow the satellite. The relative distance between test mass and a particular point of the satellite is driven to zero by the internal control system. The force needed to control the test mass is a measure of the acceleration acting on the satellite. The sensor accuracy in that mode is not as high as in the Displacement Mode but one needs no complex drag-free control algorithms as the acceleration is directly accessible.

The test mass displacement can be measured electrostatically or magnetically. In most cases, a capacitive method is used where the test mass is surrounded by electrodes. One area of the test mass and one electrode form a capacitor and the displacement induced change of its capacity can be measured, see e.g. [75].

The mode of operation depends strongly on the scientific goal of the mission. If the only purpose of the drag-free sensor is the measurement of the accelerations acting on a specific point inside the satellite in order to minimize these accelerations by a drag-free control system, the Accelerometer Mode is preferable. If on the other hand the relative displacement is needed for scientific issues or if a very high accuracy demand forbids the use of the Accelerometer Mode, the Displacement Mode should be chosen.

Currently there are two main development branches of 'state-of the-art' sensors. ONERA developed sensors like e.g. STAR flown on-board CHAMP, SuperSTAR actually flying on-board of CHAMP's successor GRACE and the GRADIO sensor on-board GOCE. All these sensors are operating in the Accelerometer Mode. Another development branch is the LTP (LISA Technology Package) currently under development at the University of TRENTO for the SMART-2 mission. This sensor is operating in the Displacement Mode where some of the axes are suspended by a suspension control system (also a accelerometer mode is foreseen). As SMART-2 is a technology demonstrator for the LISA mission the sensor must be handled as part of the experiment.

6.8. Satellite Laser Ranging

In order to measure the distance between a ground station and the satellite with very high precision the Satellite Laser Ranging (SLR) technique can be used. A very short laser pulse is transmitted from a telescope in a ground station, and it is retro-reflected by a corner cube reflector on the satellite back to the station. The round trip time is measured and gives the distance. In other words, SLR measures the absolute time of flight of photons so that the geometry of satellite and laser station can be determined precisely as long as the system calibration error is controlled to a negligible level.

It is now possible to measure travel times to accuracies of up to 50 picoseconds or better, equivalent to an accuracy of 1 centimeter or less.

Today SLR is a proven geodetic technique with significant potential for substantial contributions to studies of the Earth, Atmosphere and Oceans system. It has the ability to measure the temporal variations in the Earth's gravity field and provides an unique capability for the experimental verification of special predictions of GR. So are precise measurements of motion of near-Earth satellites and the Moon fundamental tools in the study of SR and GR and for the determination of GM, the product of the gravitational constant and the mass of the Earth. Lunar Laser Ranging using corner cube retroreflectors on the Moon has verified the UFF to 10^{-13}. As explained in section 4.2.4 and Ref. [76], SLR measurements of two satellites in special orbits has been proposed as an effective means for measuring the Lense–Thirring effect at the 1% level.

Currently NASA is building up the Satellite Laser Ranging 2000 system. SLR2000 is an autonomous and eyesafe photon-counting SLR station with an expected single shot range precision of about one centimeter and a normal point precision better than 3 mm. The system will provide continuous 24–hour tracking coverage of artificial satellites at altitudes up to 20 000 km.

Approximately forty laser station systems, distributed all over the world, now contribute to this technique. These stations form a network that is coordinated by the International Laser Ranging Service : ILRS and by an European consortium EUROLAS.

6.9. Time Transfer by Laser Link

In order to compare the time on Earth and on the satellite with high precision, a laser link should be used. The Time Transfer by Laser Link project (T2L2), developed by the Observatoire de Côte Azur [77], is in the position to compare clocks with a time stability better than 1 ps over 1000 s and better than 30 ps over 10 days. This is sufficient for the measurement of the gravitational redshift as described in the science goals. The principle is based on the propagation of light pulses between the clocks to be synchronized. Light pulses carry the temporal information from one clock to another. The ground clock has to be connected to a laser ranging station and the space clock to the T2L2 space segment. This includes a retro reflector, a time tagging unit, and a photo detection system. The station emits short light pulses in the satellite direction. The retro-reflector returns a fraction of the received photons to the ground station. The station records, for each laser pulse, the start time and the return time after reflection from the space. The T2L2 payload records the arrival time of the laser pulses. The synchronization between the clocks is obtained from all these data. With several ground stations, one can also perform a time transfer between several ground clocks in a common view or in a non-common view configuration.

6.10. Microthrusters

FEEP ion thrusters or colloidal thrusters must be used to compensate for external disturbances like solar radiation pressure acting on the satellite and disturbing its free fall behaviour, and thereby to control the residual acceleration down to 10^{-10} m/s^2 in the signal bandwidth. The first requirement sets an upper limit for the thrust: linear forces acting on the satellite are less than 50 μN in all 3 axes and maximum torques are about 10 μNm. The second condition determines the resolution of thrust control which has to be done with an accuracy of about 0.1 μN. For a satellite diameter of about 1.5 m the solar radiation pressure of about 4.4 μN/m^2 and the radiation pressure of the Earth albedo of 1.2 μN/m^2 sum up to a total drag of about 10 μN. Considering thruster noise, misalignments and other disturbing effects, a continuous thrust of 12 μN would be sufficient. To control all 6 degrees of freedom a minimum of 3 clusters of 4 thrusters is necessary. To guarantee a continuous thrust with some redundancy 4 clusters are desirable. The power consumption is less than 3 W on average with peaks up to 25 W.

6.11. Orbit

The experimental requirements define an optimum mission profile. In particular, the requirements of attitude control, maximum residual acceleration, and temperature stability result in the following specifications:

- Microthrusters like FEEPs are not effective for orbit heights less than 1000 km, because of the high gas density in lower orbits.
- To avoid charging of the capacitive reference sensor by interactions with high energy protons, highly eccentric orbits, where the satellite passes the van-Allen-belt, are not appropriate.
- The experiment testing the constancy of the speed of light requires a low perigee, because the experimental resolution depends directly on the satellite orbit velocity.
- The precise attitude control requires a star sensor with a resolution of 10 arcsec.
- Mechanical components for attitude control (e.g. flywheel or mechanical gyros) cannot be used, because of the sensitivity of the experiment to vibrations.
- Temperature stability requirements during integration times of more than 100 s can only be realized on orbits without any or with rare eclipse intervals.
- The thermal control of the satellite structure must achieve a stability of $10^{-3}\mathrm{K}/\sqrt{\mathrm{Hz}}$.

- The measurement time for tests 1 – 6 is 6 months minimum. In order to meet the scientific goals for the verification of the Lense-Thirring and the other relativistic orbital gravitational effects a minimum of 7 years tracking of the drag-free satellite is required.

Considering all experimental requirements, technological feasibility, launch capability, and design philosophy the most feasible solution is to launch the satellite in a high elliptical orbit, attainable via a geo–transfer orbit (GTO) by lifting the perigee. In this scenario, the satellite is first launched into the GTO with an apogee of 35 800 km and a perigee of only 280 km. An additional kick-motor on the satellite will lift the satellite in its final orbit with a perigee of about 10 000 km, corresponding to $\Delta v = 0.75$ km/s. A minimum height of 10 000 km enables the use of ion or colloidal thrusters and avoids flying through the van-Allen-belt. Also, the orbit eccentricity of $\epsilon \simeq 0.41$ is high enough to attain sufficient velocity differences for the constancy of the speed of light experiment. Although the relatively high orbit reduces the in–orbit velocity of the satellite by a factor of 2.8 compared to a low Earth circular orbit, it is still 20 times higher than for an Earth-based experiment.

6.12. Drag-Free and Attitude Control System

While for the coarse attitude and orbit control of the satellite rather simple sensors and control algorithms can be used, the science mode requires a more accurate control which will be applied through the Drag-Free and Attitude Control System (DFACS). For that purpose OPTIS will use drag-free sensors operating in the accelerometer mode (see Section 6.7). The drag–free control of the satellite has to make sure that the residual linear accelerations at the drag–free point are below the science requirement of 10^{-7} m/s^2.

The attitude control system of OPTIS needs to fulfill two major tasks. First, it has to ensure that the satellite's body-fixed z-axis is always pointing towards the Sun, and, second, it has to control the rotation rate around this axis very accurately. It is foreseen to use a combination of two Autonomous Star Trackers to control the attitude of the spacecraft. During experimental and safe mode, coarse attitude and orbit control are based on a sun sensor (1 arcsec resolution) and a star sensor (10 arcsec resolution). Fiber gyros are used for spin– and de–spin–maneuvers and serve to control the cold gas thrusters.

Different types of actuators have to be used for different operating modes of the satellite. Due to the nature of the experiments, a momentum wheel cannot be used so that cold gas thrusters and probably also magnetic torquers should be taken for the initial operations of the satellite (de-tumbling, Sun acquisition etc.). Again for the science mode a more accurate control is required which includes thrusters that are able to apply thrusts on the mN-level. One possibility are the Field

Emission Electric Propulsion (FEEP) thrusters which are low thrust proportional thrusters with a thrust range of 1 μN to 1 mN. Another possibility are micro-propulsion cold gas thrusters. Thanks to recent developments proportional cold gas thrusters with a maximum thrust of 0.1 mN to 1 mN (depending on the nozzle size) are now available. This second option has the advantage that it could use the same fuel as the cold gas system needed for the initial operations of the satellite [78].

Missions aiming at measuring effects at extremely low signal frequencies require a modification of the original drag-free concept because (i) no long-term experience about the performance of drag-free control systems is available and (ii) even high precision accelerometers have a very high spectral noise density near zero frequency which makes the detection of constant signals during long-term measurements impossible. Since OPTIS aims at measuring the Lense-Thirring and other relativistic effects at time scales of several years the Drag-free and Attitude Control System (DFACS) has to be able to deliver an accurate stability over that time. That is not feasible with up-to-date drag-free control systems. (It is obvious that the performance of the drag-free control system will change over the years. Due to hardware ageing effects, for example, the sensor and thruster performance will decrease.) That implies that the control parameters have to be adjusted during the mission implying the need of an In-Orbit Determination of the parameters. If changes in the controller performance occur, corrected parameters have to be determined on ground and send to the on-board computer via TC. Such an In-Orbit-Calibration procedure is in development.

7. SCIENTIFIC AND TECHNICAL OUTREACH

If the OPTIS science goals will be reached, various implications for other branches of physics this will arise—beyond the pure improvements compared with previous results:

Improvements of the Foundations of Metrology The valid definition of the meter in terms of time, and thus the present set of physical units, relies on the constancy of the speed of light. Furthermore, UGR ensures the uniqueness of timekeeping. If this universality is violated, then different types of clocks read different times in gravitational fields (which cannot be switched off). In this case, one has to restrict to one particular clock as main primary clock.

Earth Models By tracking the very precisely defined geodetic path of OPTIS, the Earth's gravitational field can be determined very precisely. This can be used to improve Earth gravity models.

Quantum Gravity All versions of quantum gravity theories like canonical or loop quantum gravity, string theory or non–commutative geometry predict

violations of the UFF, SR and the UGR. Important for the development of such quantum gravity theories is the improvement of the corresponding tests.

Clocks Clocks based on optical techniques are likely to become the most precise frequency standards in the near future. Implementing such techniques in space missions will contribute to an improved world–wide clock network of time standards (TAI). Better clocks can also improve the operating mode of GALILEO.

Furthermore, all the techniques needed for the OPTIS mission are already developed for ground use and will be of great importance for other space missions like LISA, HYPER, ASTROD, etc. Therefore, *all OPTIS technologies are key technologies* for many future space projects.

ACKNOWLEDGMENTS

We thank the German Space Agency DLR (Deutsches Zentrum für Luft– und Raumfahrt) for financial support. We also want to thank the organizers of the HYPER meeting for the invitation to present our project. Furthermore, thanks are due to C. Bordé, S. Herrmann, R. Kienzler, L. Maleki, W.-T. Ni, P. Touboul, . . . for helpful discussions.

REFERENCES

[1] Quinn, T. (1995). *Metrologia* **31**, 515.
[2] Müller, H., Herrmann, S., Braxmaier, C., Schiller, S., and Peters, A. (2003). *Phys. Rev. Lett.* **91**, 020401.
[3] Wolf, P., Bize, S., Clairon, A., Luiten, A. L., Santarelli, G., and Tobar, M. E. (2003). *Phys. Rev. Lett.* **90**, 060402.
[4] Saathoff, G., Karpuk, S., Eisenbarth, U., Huber, G., Krohn, S., Muñoz-Horta, R., Reinhardt, S., Schwalm, D., Wolf, A., and Gwinner, G. (2003). *Phys. Rev. Lett.* **91**, 190403.
[5] Turneaure, J. P., Will, C. M., Farrel, B. F., Mattison, E. M., and Vessot, R. F. C. (1983). *Phys. Rev.* **27**, 1705.
[6] Bauch, A., and Weyers, S. (2002). *Phys. Rev. D* **65**, 081101(R).
[7] Vessot, R. F. C., Levine, M. W., Mattison, E. M., Blomberg, E. L., Hoffmann, T. E., Nystrom, G. U., Farrel, B. F., Decher, R., Eby, P. B., Baughter, C. R., Watts, J. W., Teuber, D. L., and Wills, F. D. (1980). *Phys. Rev. Lett.* **45**, 2081.
[8] Ciufolini, I. (2000). *Class. Quant. Grav.* **17**, 2369.
[9] Iorio, L., Ciufolini, I., Schiller, S., Dittus, H., and Lämmerzahl, C. (in press). *Class. Quant. Grav.* **21**.
[10] Shapiro, I. I. (1990). In *General Relativity and Gravitation*, N. Ashby, D. F. Bartlett, and W. Wyss (Eds.), Cambridge University Press, Cambridge, p. 313.
[11] Fischbach, E., and Talmadge, C. L. (1999). *The Search for Non-Newtonian Gravity*, Springer-Verlag, New York.
[12] Ries, J., Eanes, R. J., and Tapley, B. D. (2003). In *Nonlinear Gravitodynamics*, R. J. Ruffini and C. Sigismondi (Eds.), World Scientific, Singapore, p. 201.
[13] Iorio, L. (2003). *Celest. Mech. Dyn. Astron.* **86**, 277.

A1

[14] Iorio, L., and Morea, A. (2004). *Gen. Relat. Grav.* **36**, 1321 (gr-qc/0304011).
[15] Iorio, L. (2002). *Phys. Lett.* **298**, 315.
[16] Lucchesi, D. M. (2003). *Phys. Lett. A* **318**, 234.
[17] Lämmerzahl, C., Braxmaier, C., Dittus, H.-J., Müller, H., Peters, A., and Schiller, S. (2002). *Int. J. Mod. Phys. D* **11**, 1109.
[18] Mansouri, R., and Sexl, R. U. (1977). *Gen. Relat. Grav.* **8**, 497.
[19] Mansouri, R., and Sexl, R. U. (1977). *Gen. Relat. Grav.* **8**, 515.
[20] Mansouri, R., and Sexl, R. U. (1977). *Gen. Relat. Grav.* **8**, 809.
[21] Will, C. M. (1992). *Int. J. Mod. Phys. D* **1**, 13.
[22] Thorne, K. S., Lee, D. L., and Lightman, A. P. (1973). *Phys. Rev. D* **7**, 3563.
[23] Haugan, M. P. (1979). *Ann. Phys.* **118**, 156.
[24] Will, C. M. (1993). *Theory and Experiment in Gravitational Physics (Revised Edition)*, Cambridge University Press, Cambridge.
[25] Ni, W.-T. (1977). *Phys. Rev. Lett.* **38**, 301.
[26] Ni, W.-T. (1984). In *Precision Measurement and Fundamental Constants II*, B. N. Taylor and W. D. Phillips (Eds.), Natl. Bur. Stand. (U.S.), Speical Publication no. 617, p. 647.
[27] Carroll, S. M., Field, G. B., and Jackiw, R. (1990). *Phys. Rev. D* **41**, 1231.
[28] Haugan, M. P., and Kauffmann, T. F. (1995). *Phys. Rev. D* **52**, 3168.
[29] Kostelecky, A., and Mewes, M. (2001). *Phys. Rev. Lett.* **87**, 251304.
[30] Kostelecky, A., and Mewes, M. (2002). *Phys. Rev. D* **66**, 056005.
[31] Lämmerzahl, C., and Haugan, M. P. (2001). *Phys. Lett. A* **282**, 223.
[32] Kostelecky, V. A., and Samuel, S. (1999). *Phys. Rev. D* **39**, 683.
[33] Ellis, J., Mavromatos, N. E., Nanopoulos, D. V., and Volkov, G. (1999). gr-qc/9911055.
[34] Ellis, J., Mavromatos, N. E., and Nanopoulos, D. V. (1999). gr-qc/9909085.
[35] Gambini, R., and Pullin, J. (1999). *Phys. Rev. D* **59**, 124021.
[36] Alfaro, J., Morales-Tecotl, H. A., and Urrutia, L. F. (2000). *Phys. Rev. Lett.* **84**, 2318.
[37] Carroll, S. M., Harvey, J. A., Kostelecki, V. A., Lane, C. D., and Okamoto, T. (2001). *Phys. Rev. Lett.* **87**, 141601.
[38] Alfaro, J., Morales-Tecotl, H. A., and Urrutia, L. F. (2002). *Phys. Rev. D* **65**, 103509.
[39] Alfaro, J., Morales-Tecotl, H. A., and Urrutia, L. F. (2002). *Phys. Rev. D* **66**, 124006.
[40] Ni, W.-T. (1973). *A Nonmetric Theory of Gravity.* Montana State University, Bozeman, MT. Available from http://gravity5.phys.nthu.edu.tw.
[41] Ni, W.-T. (1974). *Bull. Am. Phys. Soc.* **19**, 655.
[42] Colladay, D., and Kostelecky, V. A. (1997). *Phys. Rev. D* **55**, 6760.
[43] Colladay, D., and Kostelecky, V. A. (1998). *Phys. Rev. D* **58**, 116002.
[44] Ni, W.-T. (1984). In *Proceedings of the Second Asian-Pacific Regional Meeting on Astronomy*, B. Hidayat and M. W. Feast (Eds.), Tira Pustaka., Jakarta, p. 441.
[45] Müller, H., Braxmaier, C., Herrmann, S., Peters, A., and Lämmerzahl, C. (2003). *Phys. Rev. D* **67**, 056006.
[46] Lämmerzahl, C. (1998). *Class. Quant. Grav.* **14**, 13.
[47] Kostelecky, V. A., and Lane, C. D. (1999). *Phys. Rev. D* **60**, 116010.
[48] Bluhm, R., Kostelecky, V. A., Lane, C. D., and Russell, N. (2003). hep-ph/0306190.
[49] Müller, H., Herrmann, S., Saenz, A., Peters, A., and Lämmerzahl, C. (2003). *Phys. Rev. D* **68**, 116006.
[50] Haugan, M. P., and Lämmerzahl, C. (2000). *Ann. Phys.* (*Leipzig*), **9**(Special Issue SI), 119.
[51] Lämmerzahl, C., Macias, A., and Müller, H. (in preparation). *Charge Non-Conservation: A General Theoretical Frame*. **A2**
[52] Marion, H., Pereira Dos Santos, F., Abgrall, M., Zhang, S., Sortas, Y., Bize, S., Maksimovic, I., Calonico, D., Grünert, J., Mandache, C., Lemonde, P., Santarelli, G., Laurent, Ph., Clairon, A., and Salomon, C. (2003). *Phys. Rev. Lett.* **90**, 150801.

[53] Linet, B., and Teyssandier, P. (2002). *Phys. Rev. D* **66**, 024045.
[54] Lämmerzahl, C., Ahlers, G., Ashby, N., Barmatz, M., Biermann, P. L., Dittus, H., Dohm, V., Duncan, R., Gibble, K., Lipa, J., Lockerbie, N. A., Mulders, N., and Salomon, C. (2004). *Gen. Rel. Grav.* **36**, 615.
[55] Braxmaier, C., Müller, H., Pradl, O., Mlynek, J., Peters, A., and Schiller, S. (2002). *Phys. Rev. Lett.* **88**, 010401.
[56] Misner, C. W., Thorne, K., and Wheeler, J. A. (1973). *Gravitation*, Freeman, San Francisco.
[57] Ciufolini, I., and Wheeler, J. A. (1995). *Gravitation and Inertia*, Princeton University Press, Princeton.
[58] Damour, T., Piazza, F., and Veneziano, G. (2002). *Phys. Rev. D* **66**, 046007.
[59] Thirring, H., and Lense, J. (1918). *Phys. Z.* **19**, 156.
[60] Schiff, L. I. (1960). *Phys. Rev. Lett.* **4**, 215.
[61] Everitt, C. W. F., Buchman, S., DeBra, D. B., Keiser, G. M., Lockhart, J. M., Muhlfelder, B., Parkinson, B. W., Turneaure, J. P., and other members of the Gravity Probe B team. (2001). In *Gyros, Clocks, and Interferometers: Testing Relativistic Gravity in Space*, C. Lämmerzahl, C. W. F. Everitt, and F. W. Hehl (Eds.), Springer-Verlag, Berlin, p. 52.
A3 [62] Ciufolini, I. (in press). *Gen. Rel. Grav.* **36**.
[63] Ciufolini, I., Pavlis, E., Chieppa, F., Fernandes-Vieira, E., and Pérez-Mercader, J. (1998). *Science*, **279**, 2100.
[64] Iorio, L., Lucchesi, D. M., and Ciufolini, I. (2002). *Class. Quant. Grav.* **19**, 4311.
A4 [65] Einstein, A. (1975). *Sitzber. Preuss. Akad. Wiss. Berlin* 831.
[66] Lucchesi, D. (2002). *Plan. Space Sci.* **50**, 1067.
A5 [67] Rutman, J. (1978). *Proc. IEEE*.
[68] Landau, L. D., and Lifschitz, E. M. (1975). *Lehrbuch der theoretischen Physik, Vol. 7: Elastizitätstheorie*. Akademie–Verlag, Berlin.
[69] Lurje, A. I. (1993). *Räumliche Probleme der Elastizitätstheorie*, Akademie–Verlag, Berlin.
[70] Müller, H., Herrmann, S., Schuldt, T., Scholz, M., Kovalchuk, E., and Peters, A. (2003). *Opt. Lett.* **28**, 2186.
[71] Müller, H., Herrmann, S., Braxmaier, A., Schiller, S., and Peters, A. (2003). *Appl. Phys. B* **77**, 719.
A6 [72] Jornod, A., Goujon, D., Gritti, D., and bernier, L. G. (2003). *The 35 kg Space Active Hydrogen Maser (SHM–35) for ACES*.
A7 [73] Prestage, J. D., Chung, S., Burt, E., Maleki, L., and Tjoelker, R. L. (2001). *Proceedings of the 2001 IEEE International Frequency Control Symposium.*
[74] Cundiff, S. T., Ye, J., and Hall, J. L. (2001). *Rev. Sci. Instr.* **72**, 3749.
[75] Touboul, P. (2001). In *Gyroscopes, Clock, Interferometers, ...: Testing Relativistic Gravity in Space*, volume LNP 562, C. Lämmerzahl, C. W. F. Everitt, and F. W. Hehl (Eds.), Springer, Berlin, p. 274.
A8 [76] Ciufolini, I., *e al.* (1998). *LARES Phase—A Study*, Rome.
A9 [77] Samain, E., and Dalla, R. (2003). *Time Transfer by Laser Link T2L2: Micro-Satellite—Galiléo, 2003*, Observatoire Côte Azur.
[78] Schleicher, A. (2002). Technical Report, OPT-DFC-TN-ZAR-002, ZARM.

Queries to Author:

A1. Au: Please update this reference.
A2. Au: Please update this reference.
A3. Au: Please update this reference.
A4. Au: Please provide volume number, if any.
A5. Au: please provide volume number, if any.
A6. Au: Please provide adegnate details.
A7. Au: Please provide the location and the date when the proceedings were held.
A8. Au: Please provide names of all the authors.
A9. Au: Please provide publisher name and location.
A10. Au: Please note that author names are not given on the hard copy. Please check if it is typeset correctly.
A11. Au: Please Provide Table 1 citation.